# Hydrocarbon fingerprinting and palaeoenvironmental reconstruction of Cambrian-Ordovician sedimentary rocks, western Newfoundland, Canada

By

John Mishael Garcia Dooma

A Thesis Submitted to

Saint Mary's University, Halifax, Nova Scotia

in Partial Fulfillment of the Requirements for

the Degree of Bachelor of Science with Honours in Geology.

April 22nd, 2020 Halifax, Nova Scotia



Approved: Dr. G. Todd Ventura
Supervisor

Approved: Dr. Karem Azmy
External Reviewer

Date: April 22nd, 2020

# Table of Contents

# Table of Figures

## Acknowledgements

I would like to express my gratitude to Dr. Todd Ventura for the opportunity that he gave to work on an undergraduate research project. His ability to encourage excellence, endless support and his inputs to this project have been highly valuable through the completion of this thesis.

I would like to thank Dr. Karem Azmy of Memorial University of Newfoundland for giving us the opportunity to examine and look at the samples that he has been studying in a different perspective. I would like to thank Mr. Anirban Chowdhury for his assistance in doing sample preparation for this study. I would also like to thank the people of Organic Geochemistry Laboratory for giving me advice and guidance whenever I am lost doing experiments in the lab.

Lastly, my undergraduate journey has finally come to an end. I dedicate this accomplishment to my family and friends who believed in me since day one. This journey would not have been possible without everyone who helped me to become the person I am today. I thank you all from the bottom of my heart.

**Hydrocarbon fingerprinting and palaeoenvironmental reconstruction of Cambrian-Ordovician sedimentary rocks, western Newfoundland, Canada**

## Abstract

For this study, we have investigated marine carbonates and shales deposited as rhythmites from the lower Shallow Bay Formation and upper Green Point Formation of the Cow Head Group spanning the Cambrian-Ordovician boundary in western Newfoundland. Eighteen carbonate and shale samples were collected and processed for their hydrocarbon biomarkers. The resulting solvent extracts were analyzed using comprehensive two-dimensional gas chromatography-mass spectrometry (GC×GC-MS). Several petroleum biomarkers such as *n*-alkanes, acyclic isoprenoids, steranes, hopanes as well as various aromatic hydrocarbons were quantified. These compounds are used as parameters to reconstruct the paleodepositional conditions of the depositional environment, and the thermal maturation of the extractable hydrocarbons. Pristane/Phytane (Pr/Ph) ratios of the rock samples range from (~0.16 to ~3.1), indicating that the organic matter was deposited under anoxic to dysoxic and possibly oxic conditions. A comparison of the Ph/*n*-$C_{18}$ and Pr/*n*-$C_{17}$ suggests the organic matter is derived from mixed Type II/Type III kerogen. The rocks also contains $C_{27}$, $C_{28}$, $C_{29}$ αββ- and ααα-steranes 24(S+R) and αβ- and αβ-diasteranes in which the $C_{29}$ stigmastanes dominate. Gammacerane, formed from the biological precursor, tetrahymanol found in ciliated detritivores that commonly thrive in marine stratified water columns was also detected. Gammacerane Index (GI) values are low, ranging from ~0.74 to ~3.5, indicating there is minimal stratification in the water column during sediment deposition. Maturation of source rocks was assessed by monitoring the ratio of trisnorneohopane (Ts)

and trisnorhopane (Tm) as well as $C_{31}$ αβ-hopane 22S/$C_{31}$ αβ-hopane (22S+22R). Ts/(Ts+Tm) and $C_{31}$ $\alpha\beta$ S/(S+R) values are 0 to ~0.68 and ~0.45 to ~0.54, respectively. These low values indicate the organic matter in most of the samples is early to moderately mature. Samples with the highest range of Ts/(Ts+Tm) from 0.57 to 0.62 likely experienced the main phase of oil generation. The $\delta^{13}C$ profile across Shallow Bay Formation and Green Point Formation shows alternation of positive and negative $\delta^{13}C$ excursions (SPICE event, post-SPICE event, and HERB or TOCE event). Changes in organic matter ratios are observed by using steranes/hopanes and Pr/Ph ratios. Distinct negative shifts of values for the two parameters correspond to negative $\delta^{13}C_{carb}$ excursions during SPICE, post-SPICE, and HERB events. At the Cambrian-Ordovician boundary, an inverse relationship between these two parameters (high steranes/hopanes percentage accompanied by low Pr/Ph ratios) exists that may be linked to oxygen drawdown from increased productivity in the water column that affected redox conditions at depth.

Date submitted: April 22nd, 2020

# 1. Introduction

Hydrocarbon biomarkers, or molecular fossils, are determinable natural products formed from a particular biosynthetic origin that preserves in sedimentary environments (Peters and Moldowan, 2005). For palaeoenvironmental studies, the most informative hydrocarbon biomarkers are organic compounds that have a high preservation potential with a biological precursor that is structurally unique and easily identifiable when compared to other organic compounds found in sedimentary organic matter. As such, hydrocarbon biomarkers are necessarily resistant to geochemical changes (e.g., diagenesis). Biomarkers can also serve as proxies for determining the geochemical conditions of ancient environments, which can aid in the description of past organism's activities and how such activities affected the geological record (Brocks and Summons, 2003). The composition and deposition of sedimentary organic matter in a basin is environment- and time-specific as sea-level alter the composition and productivity of biota in the water column as well as the proportion of terrestrial-sourced organic matter that can be transported from the continents to the seafloor (Hedges and Keil, 1995).

For this study, three stratigraphic sections across Cambrian-Ordovician from the Cow Head Group of western Newfoundland, Canada are examined for their hydrocarbon biomarkers. Cambrian-Ordovician is a significant geologic time transition period where life started to evolve and radiate in different habitable environments. For example, the Cambrian explosion led the appearance of numerous primitive metazoans that dominated the marine environments, which some had been preserved in the fossil record (Fox, 2016; Valentine et al., 1999). In addition, primitive land plants started to radiate during the Ordovician period based on abundant and widespread spores because there are lack of

fossil record for such plants (Retallack, 2000). A petroleum biomarker study would be appropriate for this geologic time period because this would give a new perspective to observe and to investigate the fauna at a molecular scale that inhabited such environments even if the fossil record is lacking.

The Cow Head Group was nominated as the Global Boundary Stratotype Sections and Points (GSSP; Cooper et al., 2001) for the Cambrian-Ordovician boundary. The group has been exceptionally informative in terms of investigating primary stable isotope signatures in carbonates and shales used in global chemostratigraphic correlations (Azmy et al., 2014, 2015; Azmy, 2019). Outcrops of the Cow Head Group are particularly well exposed at the Martin Point Section (49º40’51”N; 57º57’36”W). In this study, organic geochemical techniques are used to characterize the carbonates and shales in the study area using hydrocarbon biomarkers. This study aims to use hydrocarbon biomarkers to describe the ancient geochemical conditions within the depositional environment and to correlate it with trace elemental measurements published by Azmy (2019) and Wang and Azmy (2019). This study will also monitor and characterize the thermal maturation of the rocks samples for hydrocarbon generation.

## *1.1. Geological Setting*

The western Newfoundland Appalachians are part of the Humber Zone, which represents a Cambrian-Ordovician passive continental margin deformed by progressive Taconic (middle Ordovician) and Acadian (Silurian-Devonian) orogenic events (Waldron and Stockmal, 1994; Bertrand et al., 2003). Active rifting on the Laurentian plate ~ 570

to 550 Ma was followed by a ca. 540 to 535 Ma rift-drift transition (Cawood et al., 2001). Continuous subsidence resulted in the initial pre-platform shelf being overlain by clastic deposits (James et al., 1989) with transgression along the Laurentian shelf margin producing thick carbonate deposits (Azmy et al., 2015; Azmy, 2019). High- to low-energy conditions were experienced by the depositional environment from the Late Cambrian to the Early Ordovician. The investigated region in this study consists of siliciclastic-carbonate slope deposits that alternate rhythmically with deep-water, non-carbonaceous to carbonaceous, organic-rich green, gray and black fissile shales and siltstones. These deposits include parted and ribbon, micritic to near-micritic, limestones and breccias derived from debris flows. Localized conglomerate beds contain marine carbonates that were transported to deep-water facies along the slope of the Laurentian margin (James & Steven, 1986; James et al., 1989; Azmy, 2019; Wang, 2019; Waldron and Stockmal, 1994). Collectively, the succession of siliciclastic muds and carbonates represent Paleo-Tethys transgression-regression fluctuations known as the Cambrian grand cycles (Lavoie et al., 2012). During rapid sea-level rises, the flooded platform formed tidal flats with shoreward-derived siliciclastic muds and shallow-marine carbonates being precipitated shelfward during the following sea-level falls (Chow and James, 1987; Spencer and Demicco, 2002).

Two formations were observed and investigated in this study (Figure 1). Shallow Bay and Green Point formations both span the Cambrian-Ordovician boundary, which also was elected as the Global Stratotype Section and Point (GSSP) defining the lower base of the Ordovician stage that is now exposed in Green Point, western Newfoundland (Cooper et al., 2001).

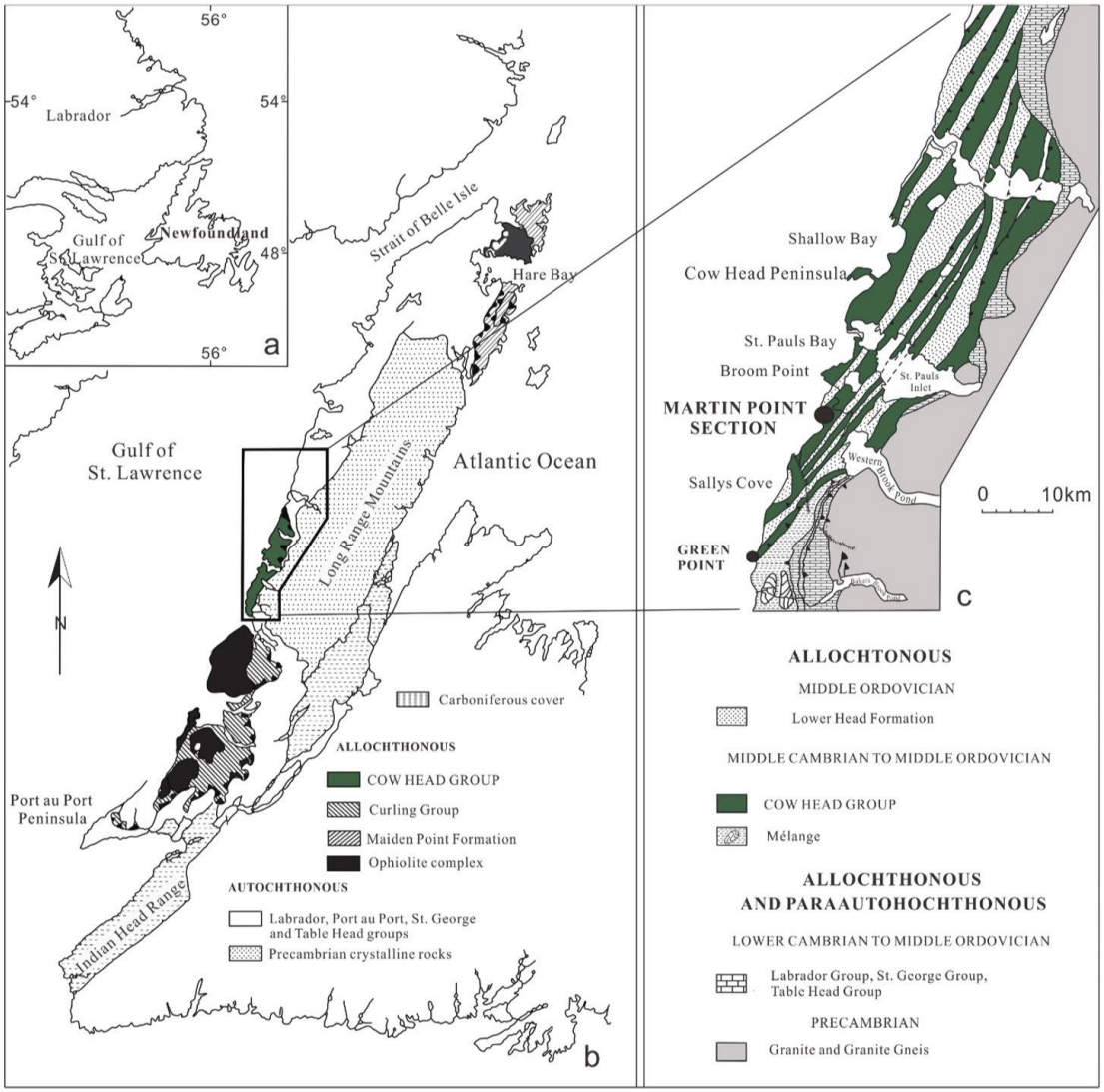


***Figure 1.*** *Surface geology map of western Newfoundland showing the research area and location of the Martin Point Section (49°40'51"N; 57°57'36"W) (from Cooper et al., 2001 and Wang, 2019).*

## *1.2. Lithostratigraphy*

### *1.2.1. Shallow Bay Formation (SBF)*

This formation mostly contains the coarser grained facies of the Cow Head Group. The Middle Cambrian basal portion of the formation is widespread and common in the area and occurring in most outcrop belts. The strata above it became more geographically restricted (James & Stevens, 1986). For this study, only one member of the Shallow Bay Formation was investigated, which is the Tucker Cove Member.

#### *1.2.1.1. Tucker Cove Member*

The Tucker Cover Member of the Shallow Bay Formation form a wide shore platform and some of the cliffs along the northern shore of the Cow Head Peninsula (James and Stevens 1986). Lithologies include black, fissile shales; parted limestone separated by green calcareous shales; well-laminated, dolomitic siltstone; calcarenite; graded-stratified conglomerate, to occasional boulder conglomerate. These strata along with the presence of carbonate turbidites have a flysch-like appearance (James and Stevens, 1986).

### *1.2.2. Green Point Formation (GPF)*

The Green Point Formation (GPF) consists of the Martin Point and Broom Point members. A detailed study of the formation was conducted by James and Stevens (1986) looking closely at sedimentology and stratigraphy of the research area. These strata are largely the fine-grained equivalent of the Shallow Bay Formation (SBF; section 1.2.1). The Martin Point and Broom Point members overlie the lower members of the SBF.

Tucker Cove Member (of the SBF) and Martin Point Member (of the GPF) are dominated by layers and lenses of limestone with a non-distinct lithostratographic boundary. The boundary is therefore placed at the transition from quartzose calcarenites of the Tucker Cove to the overlying lime mudstones of the Martin Point (James & Stevens, 1986). Green Point shales are the primary source rocks for hydrocarbon generation in the study area (Hinchey et al., 2015).

#### *1.2.2.1. Martin Point Member*

The Martin Point Member is found outside the locality section at Martin Point and these rocks occur at St. Pauls Tickle, at the base of the Green Point (Figure 2) and at The Scrape, easternmost outcrop on St. Pauls Inlet (Figure 1) (James & Stevens, 1986). The 80 to 100 m in thick rocks found in Martin Point (Wang, 2019) are green, black or gray, fissile shales with incorporation of thin layers of ribbon limestone, along with weathered siltstone and fine-grained sandstone.

#### *1.2.2.2. Broom Point Member*

The Ordovician Broom Point Member is about 90 m thick and well exposed in the study area. The rocks of Broom Point Member are distinctively a sequence of ribbon to parted lime mudstones with minor black to grey, green, fissile shale, conglomerate, and few red shale intervals. Appearance of red shales likely indicate oxygenated bottom conditions (James & Stevens, 1986). Along the succession, parted to ribbon limestones are thicker and well developed in this part of the Green Point Formation.

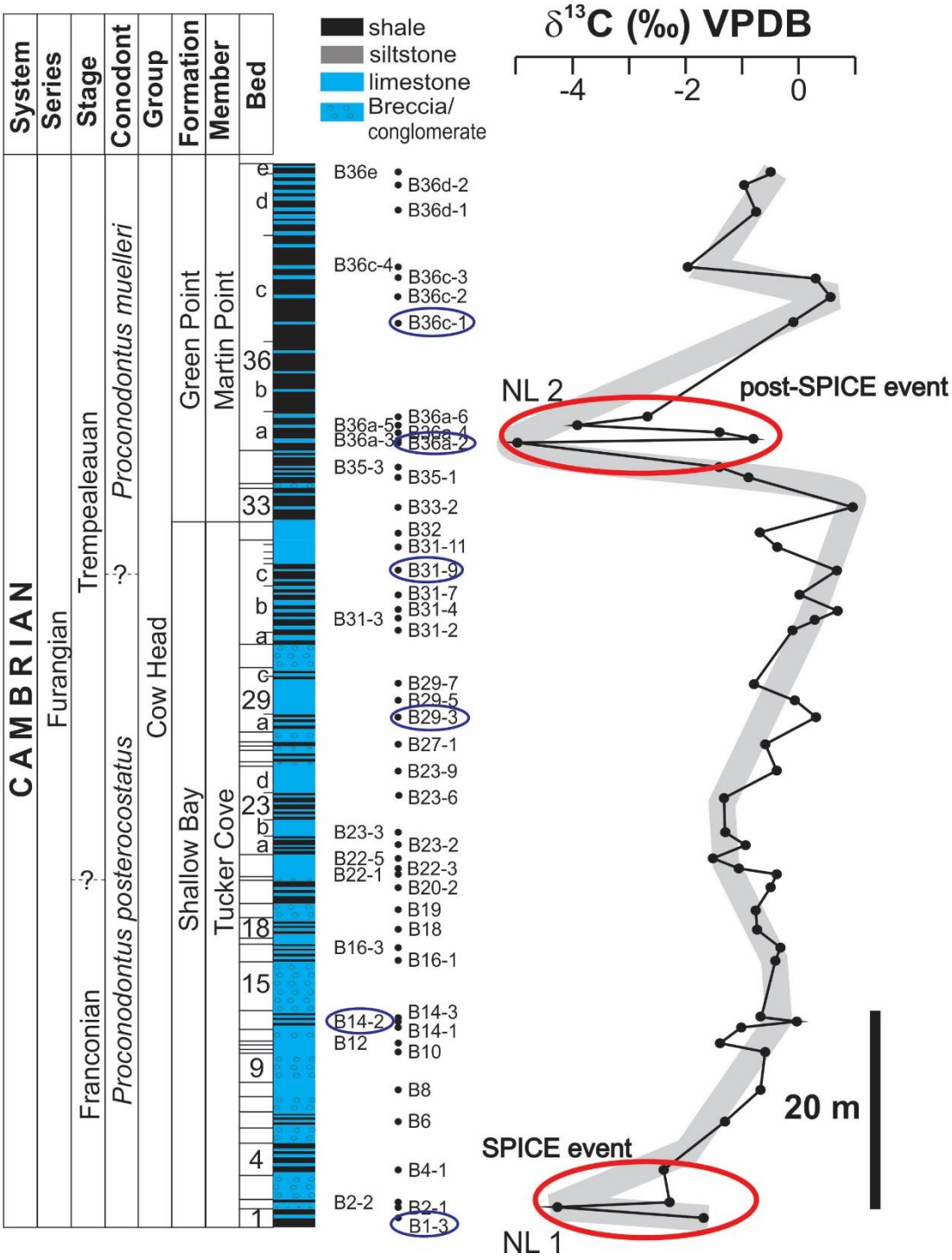


***Figure 2.*** *Stratigraphic framework of the investigated upper Shallow Bay and lower Green Point Formations in western Newfoundland showing bed number and measure positions of collected samples. Investigated samples were shown in blue ellipse. On the right-hand side, carbon isotope stratigraphy is shown corresponding to each sample (modified from Azmy, 2019).*

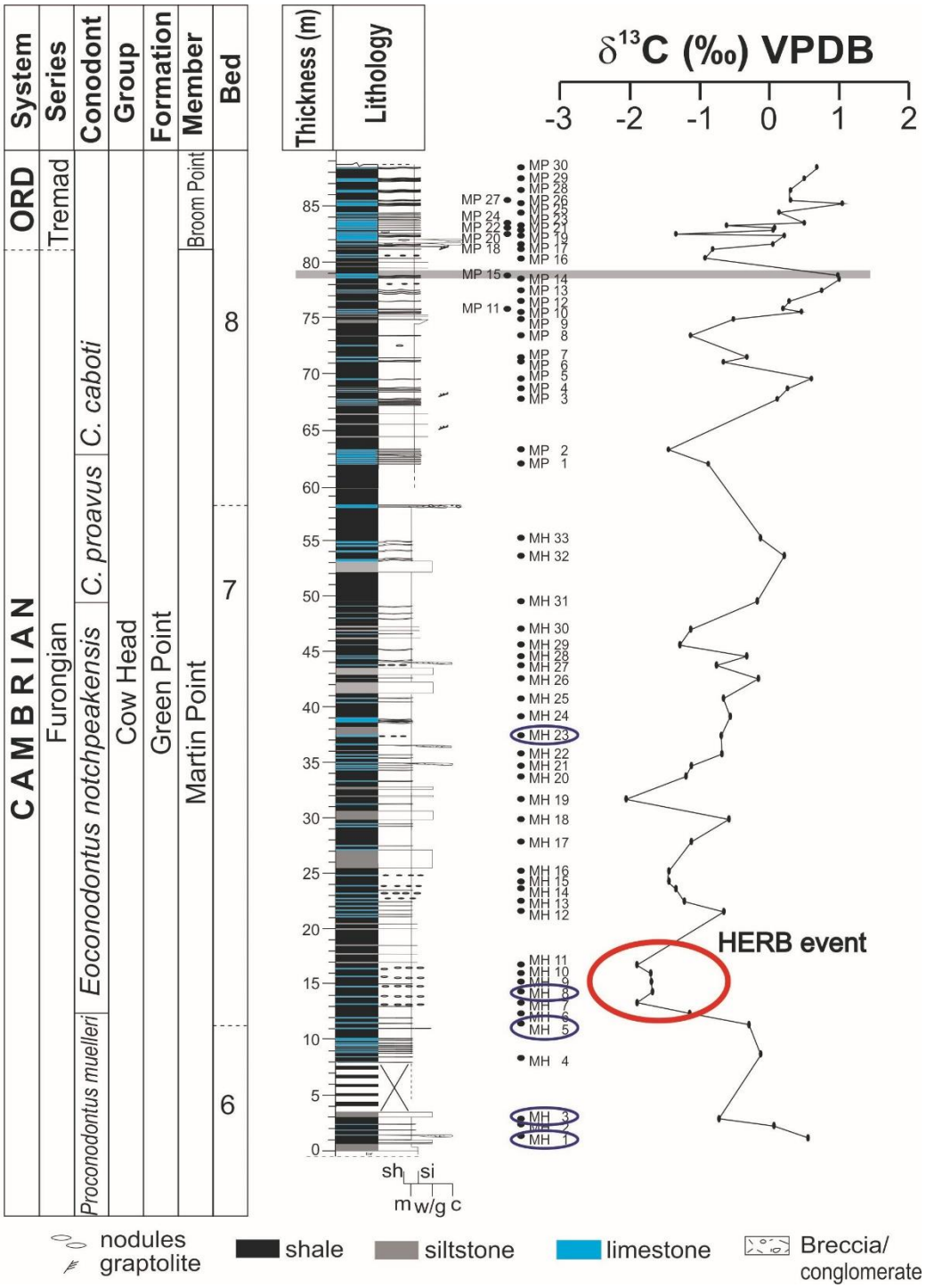


***Figure 3.*** *Stratigraphic framework of the investigated upper Cambrian Green Point Formation following Figure 2 (i.e., younger rocks). The investigated samples for their apolar extracts are highlighted by blue ellipse and their corresponding* $\delta^{13}C_{carb}$ *on the right-hand side. The solid grey line refers to the geochemical anomaly documented by Azmy et al. (2014, 2015) (modified from Azmy, 2019).*

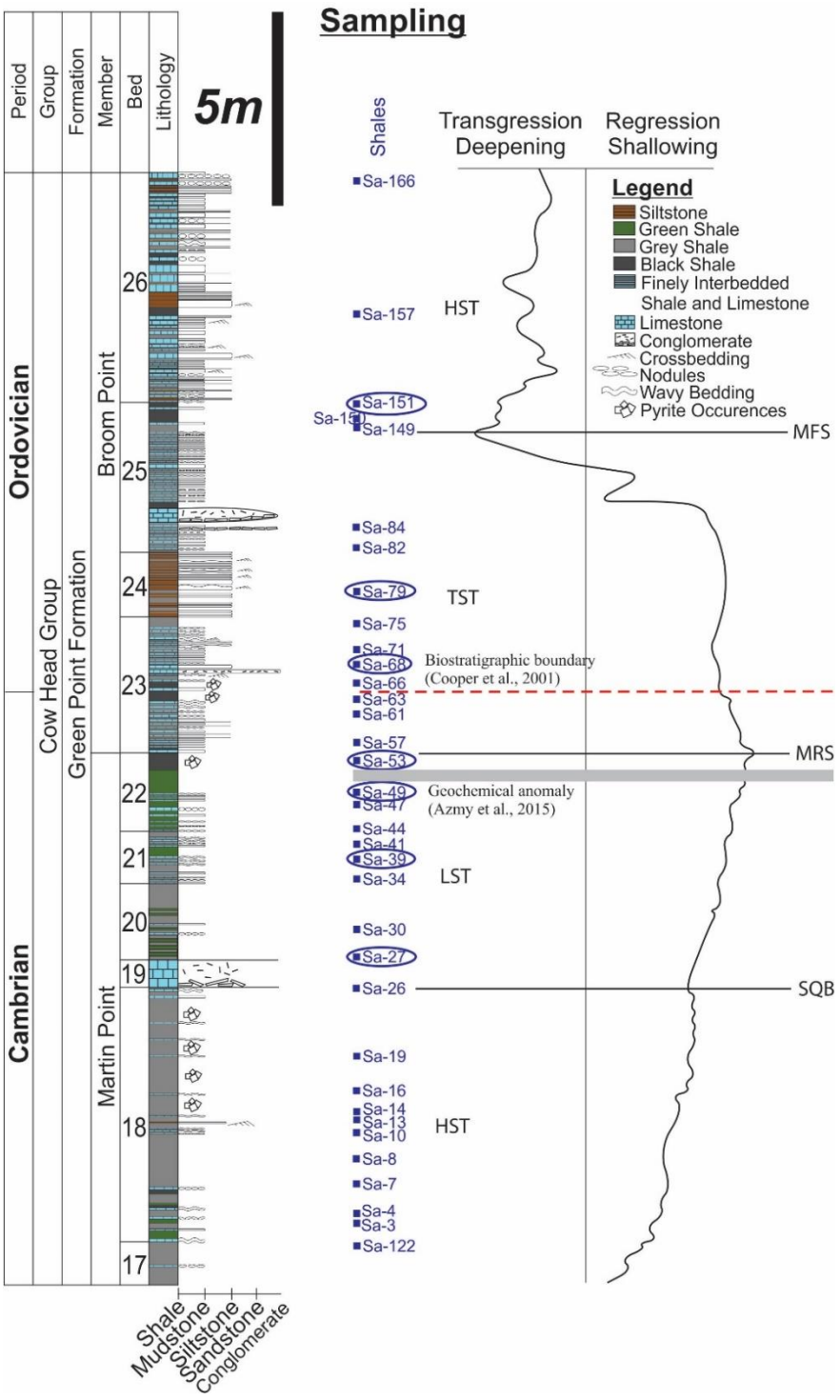


***Figure 4.*** *Stratigraphic framework of the third section, which lies on the boundary of Cambrian-Ordovician (GSSP). The samples studied are highlighted in blue ellipse and also showing reconstructed sea-level variations across the boundary. Abbreviations: HST – high stand tract; LST – low stand tract; TST – transgressive stand tract; MRS – maximum regressive surface; MFS – maximum flooding surface; SQB – sequence boundary (modified from Bisnaire et al., n.d.).*

## *1.3. Research Background*

### *1.3.1. Carbon-isotope Stratigraphy*

Azmy (2019) discussed the carbon-isotope stratigraphy in detail of Figure 2. Secular changes in C-isotopes in marine carbonates ($\delta^{13}C_{carb}$) along the strata are the result of eustatic sea-level variations during the Late Cambrian that affected primary productivity and other forms of marine biota in the ocean (Azmy, 2019; Saltzman et al., 1998; Saltzman et al., 2004; Landing, 2013). In addition, numerous potential environmental drivers that have possibly initiated these carbon isotope excursions along with the biomere extinction of trilobites that occurred in the late Marjuman to early Steptoean (LeRoy and Gill, 2019; Saltzman et al., 2000; Saltzman et al., 2015) have been reported including fluctuations in sea level (Glumac and Walker, 1998; Saltzman et al., 2004), changes in temperature (Perfetta et al., 1999; Elrick et al., 2011; Palmer, 1984), changes in ocean circulation (Saltzman et al., 2000), availability of nutrients (Saltzman et al., 2004), as well as geochemical conditions such as expanded anoxia (Palmer, 1984; Edwards et al., 2018; Saltzman et al., 1998; Saltzman et al., 2000; Saltzman et al., 2015) and euxinia in the water column (Gill et al., 2011; Dahl et al., 2014).

These $\delta^{13}C_{carb}$ excursions were global and are recorded in different parts of the world such as in Eastern Laurentia (e.g., Azmy et al., 2014; 2015; Azmy, 2018; 2019), Wa'ergang, Hunan in S. China (e.g., Li et al., 2017), Black Mountain in Australia (e.g., Ripperdan et al., 1992), Steamboat Pass in Utah, USA (e.g., Miller et al., 2014), and Quebrada de la Flecha in Argentina (e.g., Sial et al., 2008). The lowermost C-isotope excursion of the Cambrian is called the SPICE event (Steptoean positive carbon isotope

excursion). The SPICE event is correlated with a specific species of conodont, *Proconodontus posterocostatus* (see Figure 2). The post-SPICE event correlates with the *Proconodontus muelleri* Zone (see Figure 2). The HERB event (Hellnmaria – Red Tops Boundary; also known as the Top of Cambrian Excursion; Figure 3) correlates to *Eoconodontus notchpeakensis* Zone and lastly excursion of C-isotopes near the Cambrian-Ordovician boundary (James and Stevens, 1986; Azmy et al., 2014; 2015; Azmy, 2018; 2019; Cooper et al., 2001). The shifting patterns of carbon isotopes throughout the stratigraphic interval documented in these rocks records the overall simultaneous responses of temporal changes in the ocean carbon reservoir and global water chemistry. Such carbon isotope excursions, along with primary organic productivity can then be used to determine paleo-redox conditions in the depositional environment (Socorro et al., 2016, 2017; Azmy, 2018).

## *1.4. Research Objectives*

The main objective of this study is to utilize hydrocarbon biomarkers and selected trace elements geochemistry to further reconstruct the depositional and geochemical conditions of the study area during Cambrian-Ordovician times. This study also investigates if there is a correlation between hydrocarbon biomarkers and published trace element geochemical data from Azmy et al., (2014; 2015) and Azmy (2019). A secondary objective is to detect geochemical signatures across the Cambrian-Ordovician using hydrocarbon fingerprints that, if possible, can be correlated with carbon isotope excursion events (e.g., SPICE, post-SPICE, and HERB events). This study further attempts to

investigate any changes in geochemical signatures near the boundary using novel biomarker ratios. This study further focuses on the broader molecular compositions of hydrocarbon matrices extracted from specific samples using comprehensive two-dimensional gas chromatography-mass spectrometry to observe if there are additional geochemical anomaly marking chemostragraphic changes during sediment deposition. To achieve the mentioned objectives, extracted solvent from each rock powders of the samples were extracted and chemically fractionated to investigate, interpret, and quantitatively measure their hydrocarbon biomarkers. The detected biomarker groups include (1) *n*-alkanes and branched alkanes, (2) acyclic isoprenoids, (3) steroidal, (4) hopanoid, and (5) aromatic hydrocarbons.

## 2. Methodology

### *2.1. Biomarker Analysis*

Eighteen closely spaced rock samples (sampling intervals as small as 10 centimetres) were collected by Dr. Karem Azmy of Memorial University of Newfoundland that also were used in his carbon isotope studies that this project built up on (Azmy et al., 2014, 2015; Azmy, 2019). Investigated sedimentary rocks were classified based on their respective lithologies. The rock samples were characterized as limestones spanning the SPICE and post-SPICE events (labelled as B-), limestones that spanning the HERB event (labelled as MH-), and shale samples spanning the Cambro-Ordovician boundary in the GSSP at Green Point, western Newfoundland (labelled as Sa-

). Some of sample shale were interbedded with carbonate units, also known as rhythmites, which comprise slope sediments deposited under dysoxic conditions.

The total lipid extracts (TLE) were solvent extracted from rock powders using a CEM MARS 6 microwave extraction system. For each sample, 20 g of powdered rock was placed in a microwave vessel and joined with 50 mL of DCM:MeOH (7.5:1). The microwave oven ramp of up to 200 °C for 15 min at 1500 V. Three replicates of each sample extracts for each microwave extraction were combined in respective round-bottom flasks, rotary evaporated to 2 mL before being mixed with DCM:MeOH (7.5:1) and filtered using a .45μm GF filter cartridge to remove any residual sediment. The resulting TLE was transferred to pre-weighed sample vials using a Pasteur pipette column. An aliquot of the TLE was further separated into apolar and polar fractions by flash chromatography using activated silica gel (60-200 mesh) as the stationary phase in Pasteur pipette column. A solution of DCM:Hexane with a ratio of 9:1 was used to obtain the apolar fraction, which was then, followed by DCM:MeOH (ratio of 1:1) to collect the polar fraction. Elemental sulfur ($S^0$) trapped in the apolar fractions was removed by passing the sample through a column containing activated Cu (6N HCl) using hexane as the eluent.

The resulting apolar fractions were analyzed by comprehensive two-dimensional gas chromatography (GC×GC) using an Agilent 7890B gas chromatograph equipped with a Zoex Corp. ZX1 cryogenic loop jet modulator interfaced with a flame ionization detector (GC×GC-FID) that is also coupled to a Agilent 7200B quadrupole mass spectrometer (GC×GC-qToFMS). The 1$^{st}$ dimension separation was performed on a nonpolar 5% phenyl polydimethylsiloxane phase (Agilent, DB-5ms, 20.0-m; 0.25-mm

ID; 0.25-µm film thickness) and temperature programmed from 80 (held for 20 min) and ramped to 320 ºC at 2 ºC $min^{-1}$. The modulation column was a deactivated silica (1.0-m, 0.10-mm ID). The hot jet temperature programmed began at 200 ºC (held for 20 min) and then ramped to 400 ºC at 2 ºC $min^{-1}$. The $2^{nd}$ dimension separation was performed using a polar 50% phenyl equivalent polysiloxane (BPX-50, SGE, 1.5-m; 0.10-mm ID; 0.1-lm film thickness) column. A 1.0-m length 0.10-mm ID deactivated silica column was used to join the $2^{nd}$ dimension column via the capillary flow splitter into the ToF detector transfer line held constant at 230 ºC. Helium was used as the carrier gas in constant flow mode (1.2 mL/min). The GC×GC modulator period was 10 s with a 600 ms pulse duration. The qToFMS collected 50 spectra/s at 4 GHz. A detector voltage of 1800 V was used with a solvent delay of 12 min. The similar column array used for GC×GC-FID provided equivalent compound separation (Ventura et al., 2011). Quantitation of all biomarkers was performed using GC-Image software.

Quantification of all biomarkers, aromatic hydrocarbons, and organosulfur compounds was made using GC×GC-FID chromatogram using a 5α androstane internal standard. The elution pattern identification in the molecular matrix of all compounds of interest in the FID trace was determined by comparison with few samples run using GC×GC-qToFMS with the tentative identification of the specific analyte made by mass spectral analysis and also through comparing to elution position with the literature.

### *2.2. Elemental Geochemistry*

Selected trace elements concentrations used in this study were sourced from Azmy et al. (2014; 2015; 2019) and correlated with some hydrocarbon biomarker ratios. Sample preparation required digesting a subset of rock powder (~10 mg) in 2 % (v/v) $HNO_3$. The major and trace elements was analyzed using Elan DRC II ICP-MS (inductively coupled plasma mass spectrometry; Perkins Elmer SCIEX) located at Memorial University of Newfoundland. More technical details about the instrument and the standard operating procedures of the analyses can be found in journal articles published by Azmy et al. in 2014 and 2015 and Azmy in 2019.

## 3. Results and Discussion

### *3.1. Petroleum Biomarkers*

The resulting GC×GC-FID chromatogram (Figure 5) from the apolar extracts display groups of organic molecules. These compounds include *n*-alkanes and branched alkanes, acyclic isoprenoids, alkylcycloalkanes, and cyclic terpenoids. Cyclic terpenoids included tricyclic (e.g., cheilanthanes), tetracyclic (e.g., steranes), and pentacyclic (e.g., hopanes) terpanes. Additionally, the samples also contain a broad array of aromatic compounds that include alkylbenzenes, naphthalenes, and phenanthrenes. Common organosulfur compounds, such as benzothiophenes and dibenzothiophenes, were of low abundance and typically below detection limits.

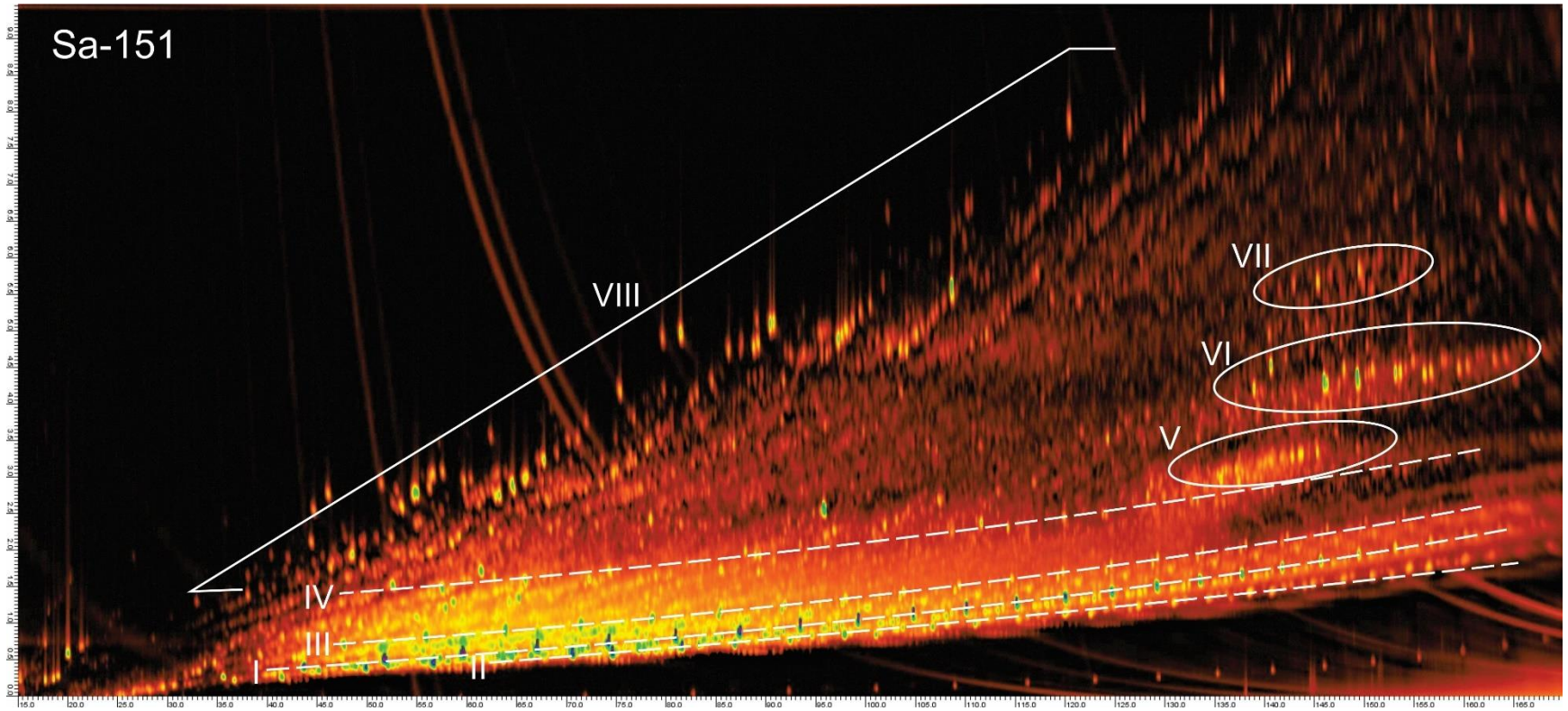


***Figure 5.*** *Example of a GC×GC-FID chromatogram from an apolar extract of shale sample Sa-151 (see Figure 4). The dotted lines indicate the elution pattern of the molecular matrix. (I) n-Alkanes and branched alkanes, (II) acyclic isoprenoids, (III) alkylcycloalkanes, (IV) alkylbenzenes and tricyclic terpanoids, (V) steranes, (VI) hopanoids, and (VII) triaromatic steroids, (VIII) aromatic hydrocarbon biomarkers.*

### *3.1.1. Normal Alkanes and Acyclic Isoprenoids*

Each sample from the Cow Head Group (comprising of the Shallow Bay and Green Point formations) contains homologous series of *n*-alkanes ranging from *n*-$C_{12}$ to *n*-$C_{36}$ and acyclic isoprenoids, such as norpristane (*i*-$C_{18}$), pristane (Pr or *i*-$C_{19}$), and phytane (Ph or *i*-$C_{20}$). The distributions of *n*-alkanes are significantly different (Figure 6) between lithologies. Carbonates of the SPICE event (B-series) have higher abundance of *n*-alkanes; with two samples, B1-1 and B31-9, notably having a broader abundance than the rest. The carbonates of the HERB event (MH-series) have a relatively low concentrations of *n*-alkanes compared to the latter group of samples, but the samples are following similar trend in terms of their distribution based on their relative *n*-alkane concentration (ng/g). This may suggest the possibility of biomarker syngeneity in the HERB carbonate sample set (Ferrer et al., 2018). The shales spanning the Cambrian-Ordovician boundary (Sa-series) exhibit a similar trend of distribution of *n*-alkanes. However, shale sample Sa49, sourced below the Cambrian-Ordovician boundary, shows an increase in *n*-$C_{15}$ and Ph values among other shales.

Carbon preference index (CPI) can be used to measure the degree of terrestrial sourced higher plant waxes that have odd predominance of higher molecular weight *n*-alkanes (Eglinton and Hamilton, 1967; Douglas and Eglinton, 1966). This proxy can also be used to track the maturation of organic matter. As source rocks become heated with deeper burial, the CPI associated the source rock bitumen's will decrease due to cracking. CPI values that are greater than one therefore indicate the organic matter in the source rocks is immature. Several samples in the study area have CPI values near one suggesting the organic matter in the rocks are of have higher maturity (Figure 7, Table 4).

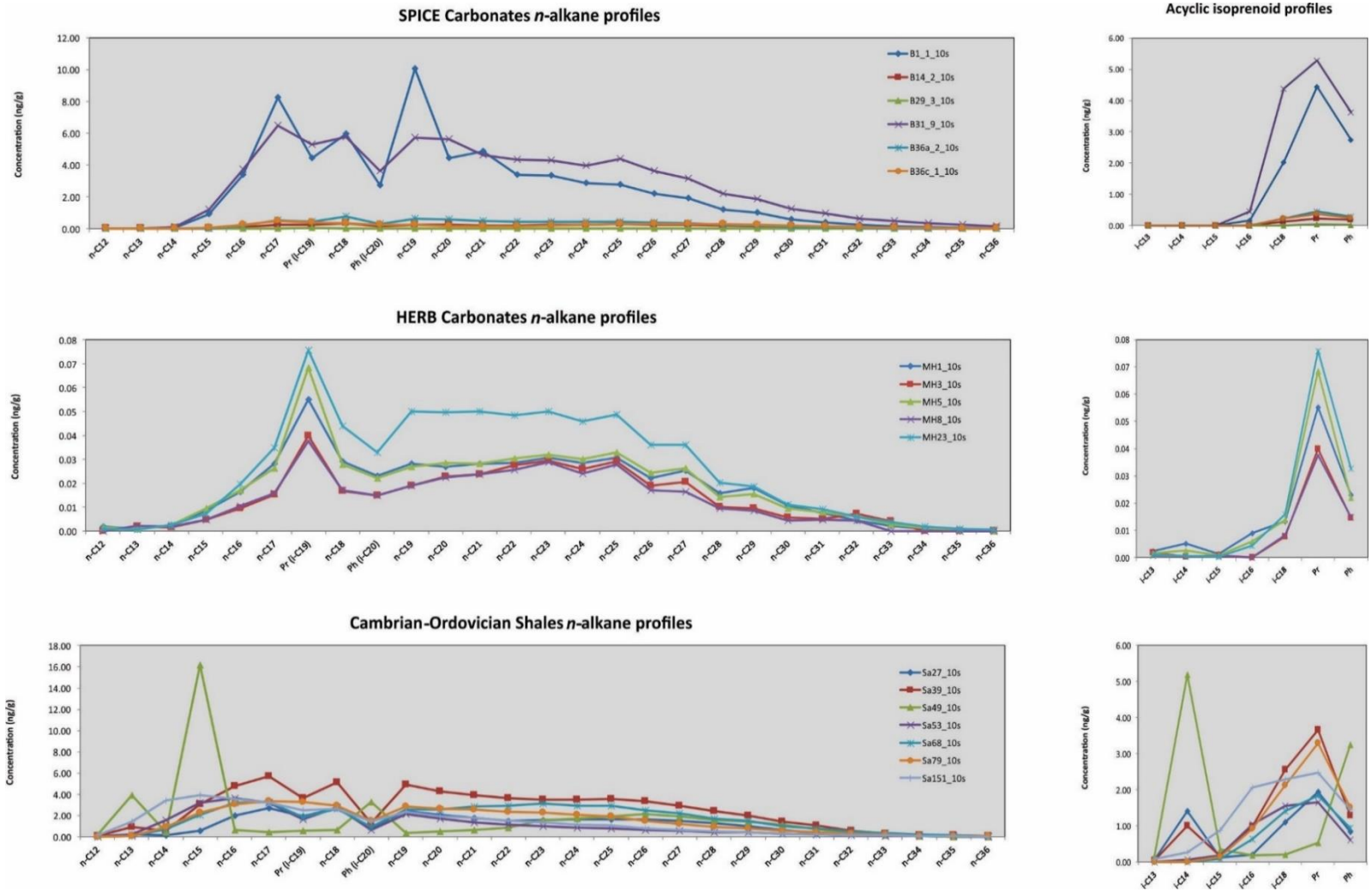


***Figure 6.*** *Concentration of n-alkanes and its corresponding acyclic isoprenoid profiles of shales and carbonates of the study area. The similar mono-modal profiles indicate organic matter syngeneity.*

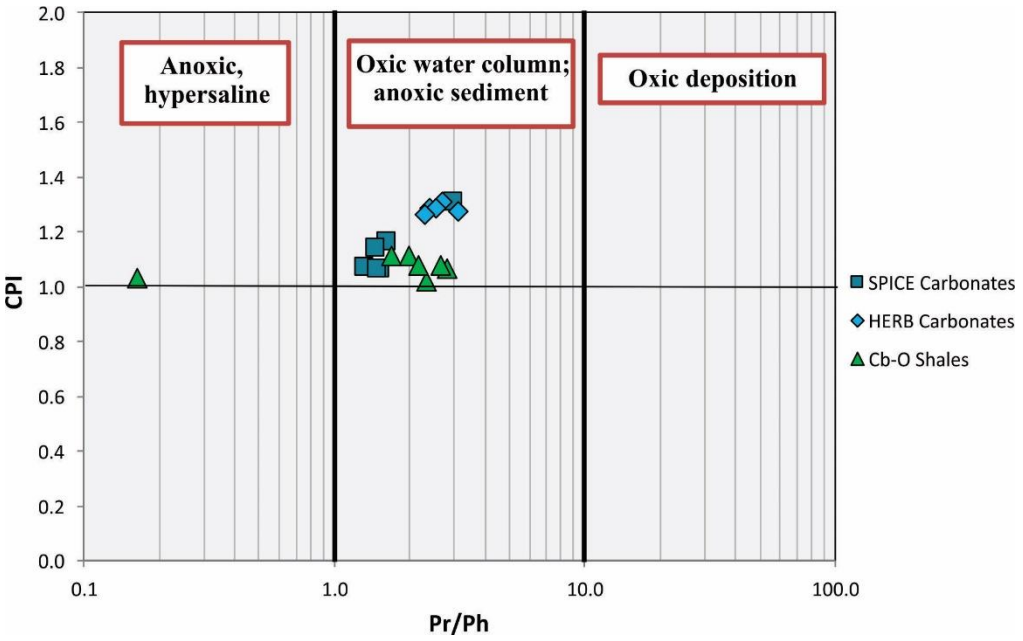


***Figure 7.*** *Cross-plot of Pr/Ph versus CPI. All samples have low CPI indicating they do not have significant contributions of thermally immature higher plant waxes. Pristane and phytane ratios suggest the sediments were deposited in dysoxic to oxic conditions.*

Pristane (Pr) and phytane (Ph) are both abundant biomarkers in petroleum source rocks and also important molecular indicators for palaeoenvironmental studies. These organic molecules can be sourcing from different organisms. Phytane is commonly considered to be sourced from phytol, which is derived from phytyl the major side-chain of chlorophyll *a*. Pristane is formed by oxidation and decarboxylation of phytol whereas Phytane (Ph) develops by reduction and dehydration of phytol (Powell and McKirdy, 1973). In other words, phytol has undergone differential oxidative and reductive steps that can interpret the redox conditions of the ancient depositional environment (Didyk et al., 1978; Sefein et al., 2017). Therefore, the Pr/Ph ratio is frequently used as a paleo-redox measure in paleoenvironment studies. High Pr/Ph ratios will indicate sediment deposition in fully oxic conditions. Peters et al. (2005) suggested that high Pr/Ph ratios

(>3) indicate the deposition of terrestrial organic matter was under oxic conditions. Low Pr/Ph ratio mark sediment deposition in dysoxic to anoxic conditions (<3). Most of the carbonate and shale units are deposited in dysoxic/suboxic conditions, and particularly, one shale unit plots in anoxic zone based on low Pr/Ph value (Figure 7, Table 4). Additionally, Pr/*n*-$C_{17}$ and Ph/*n*-$C_{18}$ ratios (Figure 8) can compliment results shown by Pr/Ph, and the ratios provides constrain on both redox conditions and the type kerogens giving rise to the source rock bitumens. In terms of kerogen types, HERB carbonates are described as type III, that indicates terrigenous-sourced organic matter deposition, whereas SPICE carbonates and Cb-O shales are type II/III kerogen, indicating mixed source of organic matter. (Figure 8, Table 4).

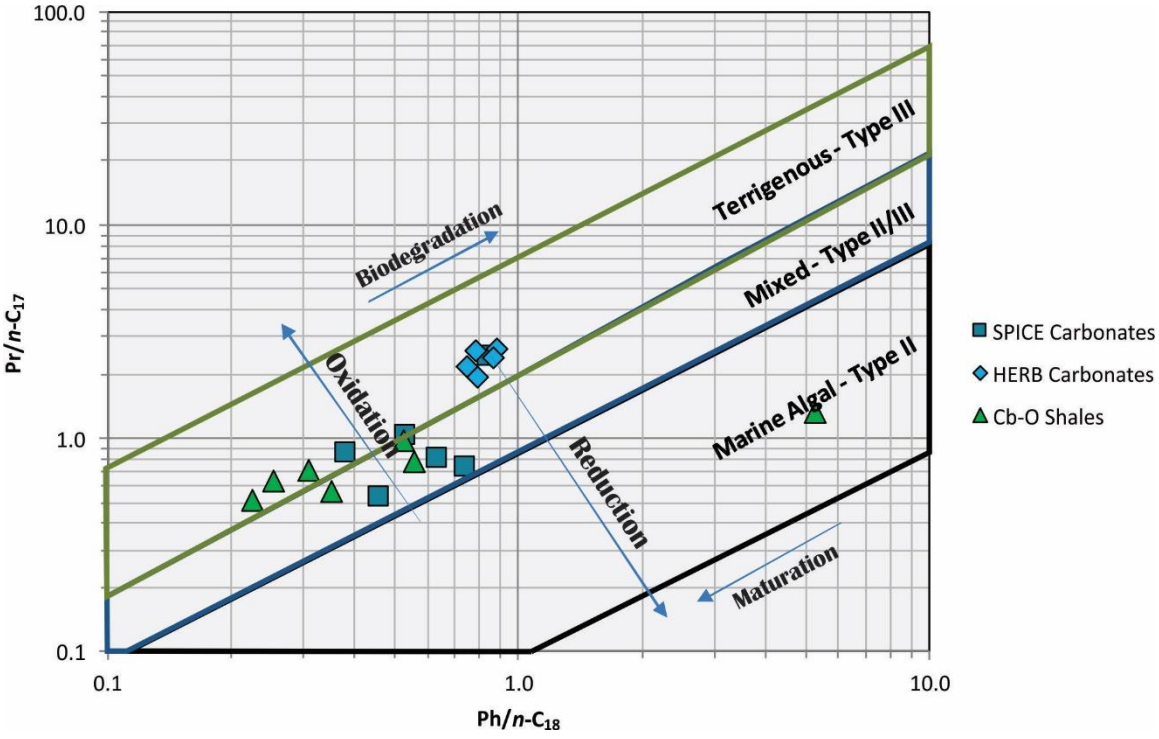


***Figure 8.*** *Cross-plot of Ph/n-$C_{18}$ versus Pr/n-$C_{17}$. SPICE, HERB carbonates and Cambro-Ordovician shales appear to have a mix of marine and terrestrial input of organic matter. Most kerogen types are types II, II/III, and III. One marine Cb-O shale sample is particularly rich in algal material. HERB carbonates are all type III kerogen.*

### *3.1.2. Steroid Biomarkers*

Steroidal biomarkers were monitored using the 217 and 218 *m/z* extracted ion chromatograms from samples analyzed by GC×GC-ToFMS. The identified compounds were then mapped to GC×GC-FID chromatograms and the calculated their peak intensities was used to quantitate absolute lipid abundances. Regular steranes indicate eukaryotic inputs of organic matter to the source rocks (Peters et al., 2005). All of the carbonates and shales from the study area contain regular steranes that range in carbon number from $C_{22}$ to $C_{29}$. The concentration of regular sterane increases with carbon number (i.e., $C_{27}<C_{28}<C_{29}$) (Figure 9, Table 5). All of the samples show higher abundances of $C_{29}$ regular steranes (avg. 57.3%) relative to $C_{28}$ ergostanes (avg. 27.7%) and $C_{27}$ cholestanes (avg. 15.0%). Two of the HERB carbonate units, MH3 and MH8, contain very low abundance of such steranes (i.e., below detection limits).

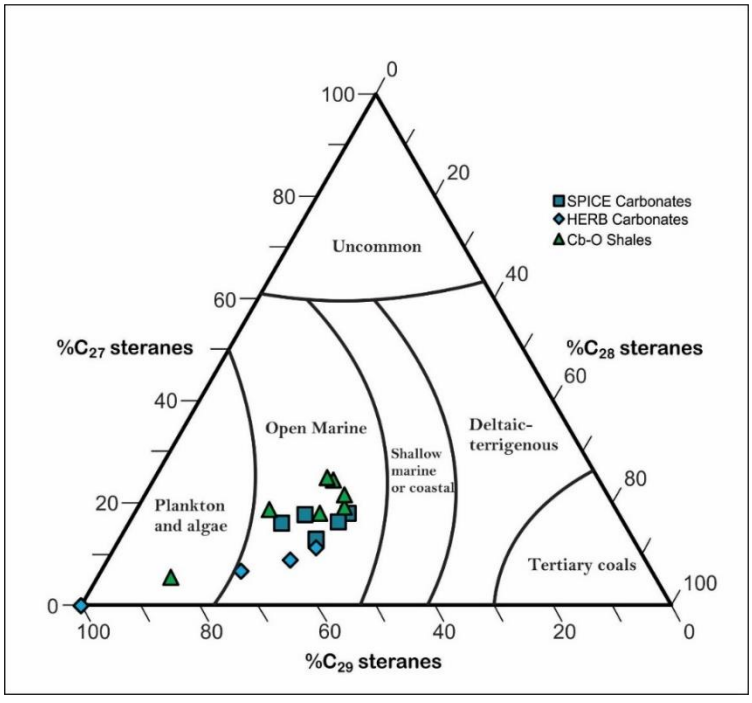


***Figure 9.*** *Ternary diagram of regular steranes including cholestane ($C_{27}$), ergostane ($C_{28}$), and stigmastane ($C_{29}$). The relative abundance of these three homologs indicate the host*

*organic matter was sourced from open marine environments that could be rich in plankton and algae (modified from Fang et al., 2019).*

The $C_{29}$ stigmastanes are predominately sourced from 4-desmethyl sterols that are commonly found in higher plants and marine unicellular algae (Volkman, 1986). Caution should be taken with regards to indication of sources of organic matter and should be supported by other novel biomarker data as such type of sterols, which are sources of steranes, are common membrane constituents in land plants and marine algae. However, in ancient sediments, high concentrations of $C_{29}$ steranes indicate that organic matter was not derived from vascular plants (i.e. rocks of Cambrian-Ordovician age), as vascular plants had not invade terrestrial environments until the Late Ordovician (Volkman, 1986; Summons and Walter, 1990; Huang and Meinschein, 1979; Moldowan et al., 1985; Salamon et al., 2018).

Rearranged steranes are present as $C_{27}$ to $C_{29}$ αβ-diasteranes. The relative proportion of rearranged to regular steranes is lithologically controlled. Most of these diasteranes are abundant in siliciclastic Cambrian-Ordovician shales, indicating $C_{27}$ to $C_{29}$ regular steranes have undergone acid clay catalysis during sedimentary organic matter diagenesis (Johns, 1979). Some of the carbonate units also indicate the presence of diasteranes, which may also possibly indicate inputs of clay minerals during carbonate cementation.

### *3.1.3. Hopanoid Biomarkers*

Hopanoid biomarkers were monitored using the 177, 191, and 205 *m/z* extracted ion chromatograms from samples analyzed by GC×GC-ToFMS. The identified compounds were then mapped to GC×GC-FID chromatograms and their peak intensities were calculated to quantitate absolute lipid abundances. Bacterial hopanoid biomarkers were detected in all samples. Hopanoids were dominated by high abundance of $C_{29}$-norhopane, $C_{30}$-hopane, gammacerane, and series of homohopanes from $C_{31}$ to $C_{35}$. These bacterial inputs relative to eukaryotic inputs are lithologically specific. The SPICE and HERB carbonate units (avg. 24.9% and 19.2%, respectively) have relatively lower sterane/hopane ratios compared to the siliciclastic shales near the Cambrian-Ordovician boundary (avg. 48.1%). This suggests a larger bacterial influence during carbonate cementation. The concentration of $C_{29}$ αβ-norhopane relative to $C_{30}$ αβ-hopane has been widely used to determine paleoenvironment of oils either from siliciclastic (>0.5) or marine carbonate environments (<0.5). Most of the samples from this study sit in the siliciclastic field.

Gammacerane is present and highly abundant in all of the carbonate and shale units in this study. Gammacerane is believed to have originated from the hydrocarbon skeleton of tetrahymanol, which is found in bacterivorous marine ciliates and photosynthetic sulphur bacteria *Rhodopseudomonas palustris* (Kleemann et al., 1990). The pathway for the formation of gammacerane is most likely by reduction of tetrahymenol followed by subsequent hydrogenation during diagenesis (Peters et al., 2005; ten Haven et al., 1989; Sinninghe Damsté et al., 1995; Venkatesan, 1989; Harvey and Mcmanus, 1991). The Gammacerane index [GI = (gammacerane ×

10)/(gammacerane + $C_{30}$ αβ-hopane)] is used as a proxy for the evaluation of water column stratification during sediment deposition. All of the samples show low GI values (avg. 1.66) that indicate mild stratification in the water column. The carbonate units show a range of GI values, which are both correlated to the ratio of $C_{28,30}$-bisnorhopane to $C_{30}$ αβ-hopane [BNH/(BNH + $C_{30}$ αβ-hopane)] that possibly suggests redox condition changes in the water column may be linked to water column stratification (Figure 10).

The presence of 2α- and 3β-methylhopanes were monitored using the *m/z* 205 extracted ion chromatograms. The biological precursors of 2α-methylhopanes are believe to be 2- methylbacteriohopanepolyols that are commonly found specific to oxygenic cyanobacteria, like such that compose stromatolites as old as 2.7 Ga (Summons et al., 1999; Peters et al., 2005; Farrimond et al., 2004; Matys et al., 2019). Other precursor of 2α-methylhopanes can also be anoxygenic phototroph such as *Rhodopseudomonas palustris*, by deriving $C_2$ methyl group from methionine to biosynthesis of 2-methylbacteriohopanepolyols (Rashby et al., 2007; Summons and Walter, 1990). The presence of 2α-methylhopanes can be quantified via the use of 2α-methylhopane index [2α-MHI = $C_{31}$ 2α-methylhopane/($C_{31}$ 2α-methylhopane + $C_{30}$ αβ-hopane)] that determine loading of nutrients in the ancient environment. All of the samples have low 2α-MHI values and are negatively correlated with GI. The 2α-MHI values of SPICE and HERB carbonates ($R^2$ = 0.10 and 0.92, respectively) are positively correlated to the sterane/hopane ratio, but 2α-MHI of Cambrian-Ordovician shales are negatively correlated. This may suggest low algal competition on the biological oxygen demand in the water column and sediments.

The series of 3β-methylhopanes are also detected in most of the carbonate and shale units. 3β-methylhopanes are believed to originate from the biological precursors 3β-methylbacteriohopanepolyols that are derived from methanotrophic bacteria and some aerobic acetic acid bacteria (Farrimond et al., 2004; Welander and Summons, 2012). *Methylococcus capsulatus* and *Methylomonas methanica* are examples of methanotrophic bacteria that synthesize regular hopanoids and 3β-methylated hopanoids, which can be source of 3β-methylhopanes in sediments (Summons et al., 1994; Neunlist and Rohmer, 1985; Welander and Summons, 2012). The presence of 3β-methylhopanes can indicate lacustrine conditions that might represent methanotrophic bacterial activity in the depositional environment (Farrimond et al., 2004). Similar to 2α-methylhopanes, 3β-methylhopane abundances can be measured using the 3β-methylhopane index [3β-MHI = $C_{31}$ 3β-methylhopane/($C_{31}$ 3β-methylhopane + $C_{30}$ αβ-hopane) that can indicate methanotrophy or lacustrine environment (Figure 10). For SPICE and HERB carbonate units, the 3β-MHI is positively correlated ($R^2$ = 0.65 and 0.23, respectively) to sterane/hopane ratio indicating increasing lacustrine conditions are associated with increasing inputs of algae (Figure 10).

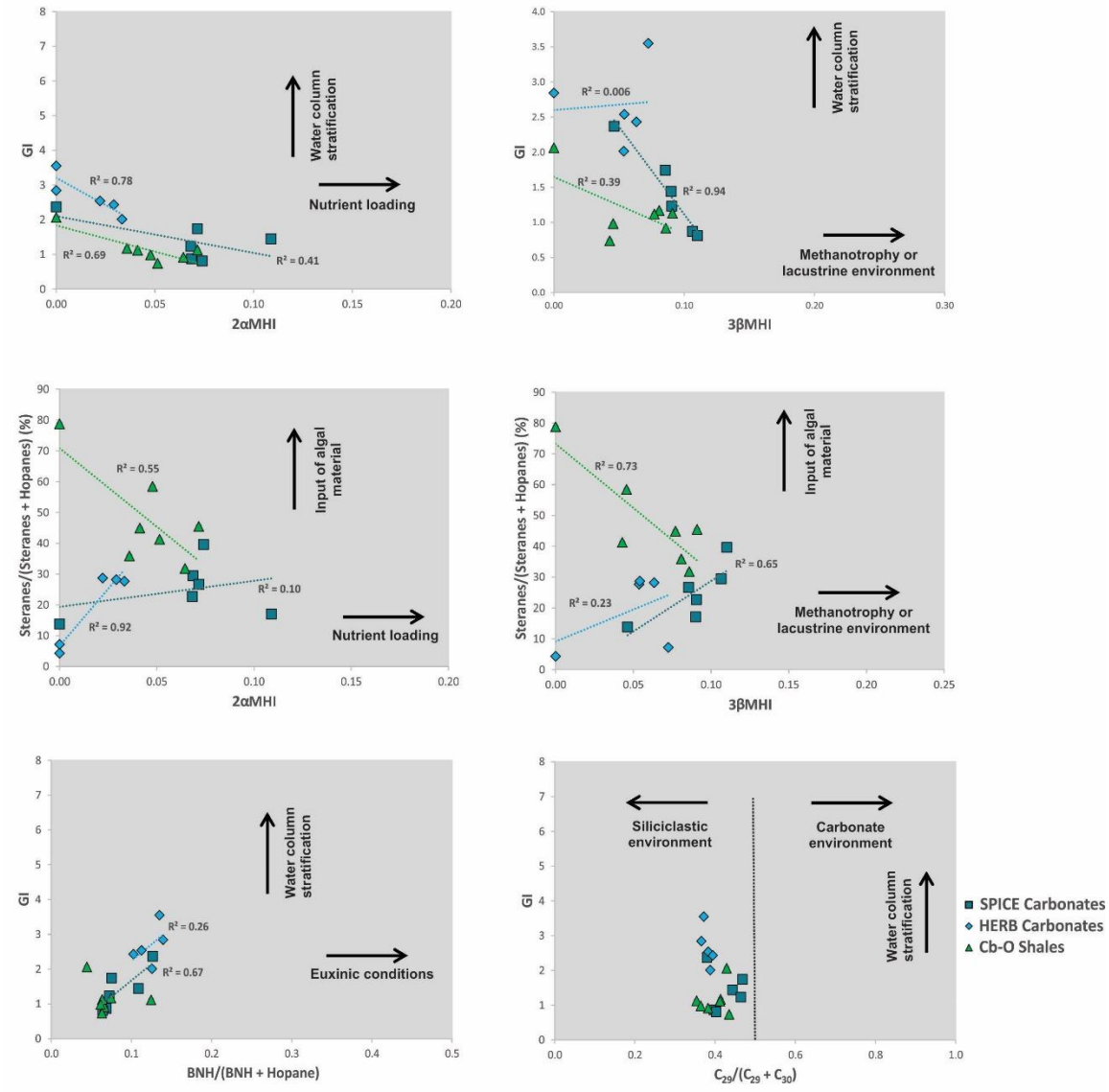


***Figure 10.*** *Cross-plots of various novel hopanoid biomarkers. Gammacerane index is a proxy to indication of water column stratification. The 2α- and 3β-methylhopane indices indicate presence of oxygenic photosynthesis and methanotrophic activity. The sterane/hopane ratio is the index for measuring relative proportions of bacterial to eukaryotic organic matter, predominantly input of algal material (modified from Ventura and MacRae, 2019).*

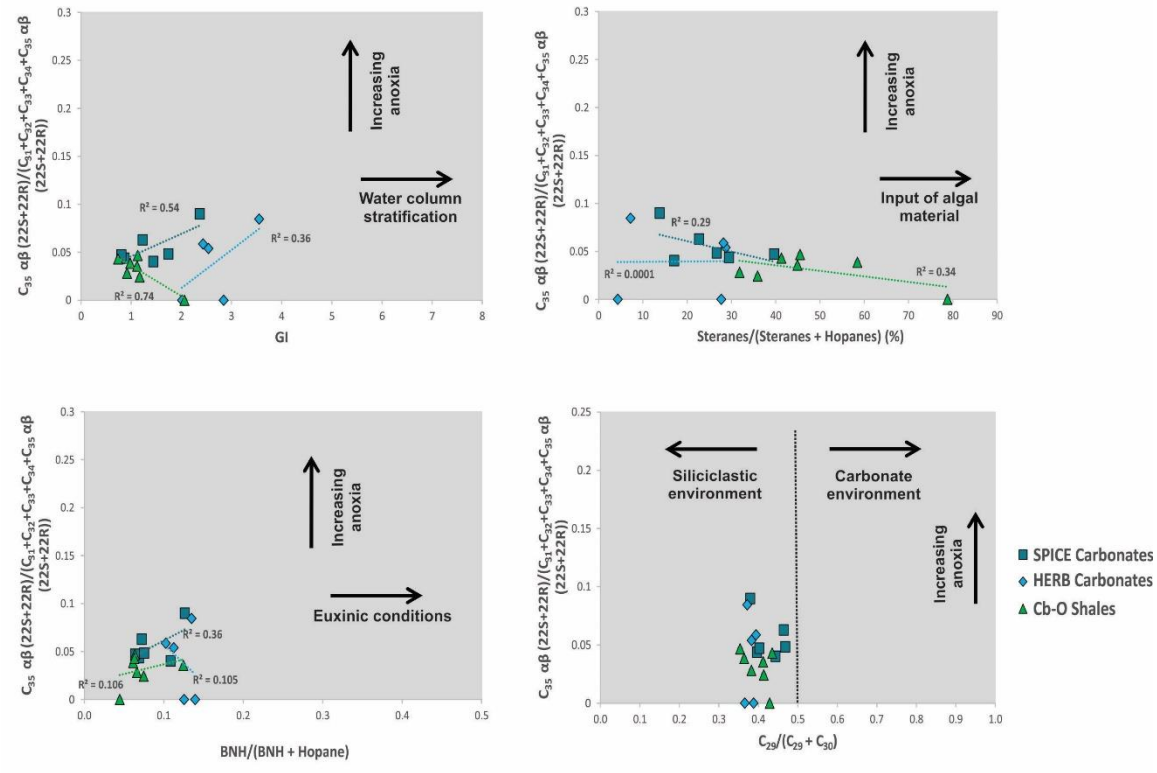


***Figure 11.*** *Cross-plots of homohopanes versus other hopane biomarkers. Homohopanoid biomarkers are used to indicate the degree of anoxic conditions in the water column (Peters et al., 2005).*

The series of $C_{31}$- to $C_{35}$-homohopane are also detected and quantitated in the samples. Homohopanes are thought to have originated from bacteriohopanetetrol and possibly other polyfunctional $C_{35}$ hopanoids that are commonly biosynthesized by prokaryotic organisms (Peters et al., 2005; Ourisson et al., 1984; Ourisson et al., 1979; Rohmer et al., 1991). High $C_{35}$-homohopane indices are diagnostic of petroleum source rocks deposited under marine anoxic conditions (Peters and Moldowan, 1991). The $C_{31}$- to $C_{35}$- can be quantitated using the $C_{35}$-homohopane index [$C_{35}$-HH Index = $C_{35}$ αβ (22S+22R)/($C_{31}$+$C_{32}$+$C_{33}$+$C_{34}$+$C_{35}$ αβ (22S+22R))]. This index can then be plotted against gammacerane index (degree of water column stratification), sterane to hopane ratio (input of algal material), bisnorhopane to hopane ratio (degree of euxinia), and $C_{29}$-

norhopane to $C_{30}$-hopane ratio (siliciclastic or carbonate depositional environment). None of the Cow Head Group samples show exceptionally high values of $C_{35}$-homohopane indices, which suggest that the sediment deposition occurred in dysoxic/suboxic environment, as it could have resulted from the suboxic exposure leading to partial oxidation of the bacteriohopanetetrol side chain (Peters and Moldowan, 1991), and also previously indicated by Pr/Ph (section 3.1.1.).

### *3.1.4. Tricyclic Terpanoid (cheilanthanes) Biomarkers*

Tricyclic terpanes were monitored using the *m/z* 123 and 191 from extracted ion chromatograms. Tricyclic terpanes were present in most carbonate and shale units and ranged from $C_{20}$ to $C_{33}$ except in samples MH3, MH8, and Sa-49, where such terpanes were close to detection limits. Tricyclic terpanes appear to originate from tricyclohexaprenol formed from the cyclization of hexaprenol (Heissler and Ladenburger, 1988) and could be constituents of prokaryotic membranes (Peters et al., 2005; Moldowan et al., 1983; Krajewski-Bertrand et al., 1990). High concentrations of tricyclic terpanes have been reported and correlated with primitive green algae *Tasmanites* as algal source (Greenwood et al., 2000; Dutta et al., 2006). The abundance of these compounds are consistent with a late release from kerogens that are thermally mature (Farrimond et al., 1999).

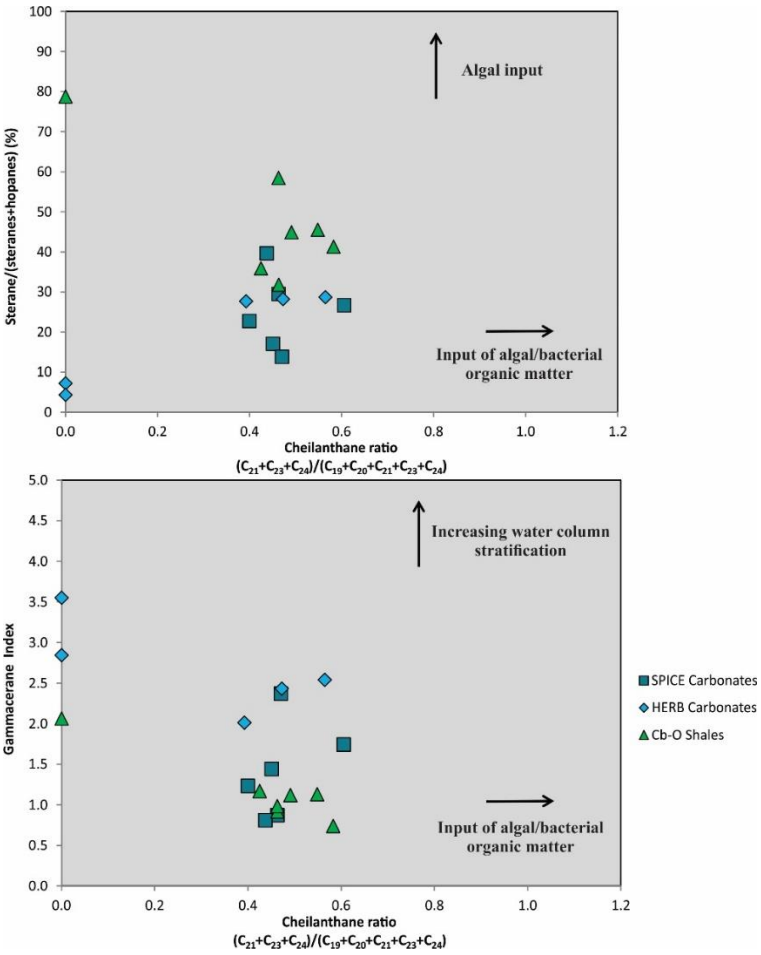


***Figure 12.*** *Cross-plots of tricyclic terpenoids versus sterane/hopane ratio and GI. The sterane/hopane ratio is the quantitative measure of proportions of bacterial to eukaryotic inputs of organic matter, dominantly algal source. Gammacerane index is the measure of the stratification in the water column.*

### *3.2. Thermal Maturity of Sedimentary Organic Matter*

Thermal maturity is the extent to which heat-driven reactions have modified the structure and composition of organic matter – typically involving its conversion to oil and gas. In relation to diagenesis, early diagenetic processes convert bacterial and plant inputs of organic matter to kerogen and bitumen (Peters et al, 2005; Baskin, 1997). Various biomarkers such as hopanes and steranes were used to determine the thermal maturation of the source rocks in the study area. For example, moretanes are thermally less stable

than $C_{30}$ hopanes and its abundance decreases with increasing thermal maturity (Seifert and Moldowan, 1980). The ratio of moretane ($C_{30}$ βα) to hopane ($C_{30}$ αβ) averaged 0.21 for the sample set indicating that the organic matter is thermally mature. Hopane ratios $C_{31}$ αβ-hopane 22S/$C_{31}$ αβ-hopane (22S+22R) averaged 0.56 (Figure 12, Table 5). Ratio of trisnorneohopane (Ts) and trisnorhopane (Tm) [Ts/(Ts + Tm)] was assessed as $C_{27}$ 17α-trisnorhopane is less stable than $C_{27}$ 18α-trisnorneohopane (Seifert and Moldowan, 1978), which for the Cow Head Group averaged 0.41. For steranes maturity parameters, the ratios $C_{29}$ ααS/$C_{29}$ αα(S+R) and $C_{29}$ ββ (S+R)/($C_{29}$ ββ (S+R) + $C_{29}$ αα(S+R)) averaged 0.44 and 0.51, respectively. Using these parameters, the sedimentary organic matter in the potential source rocks are ranging from early mature to mature (Seifert and Moldowan, 1978; Peters et al., 2005).

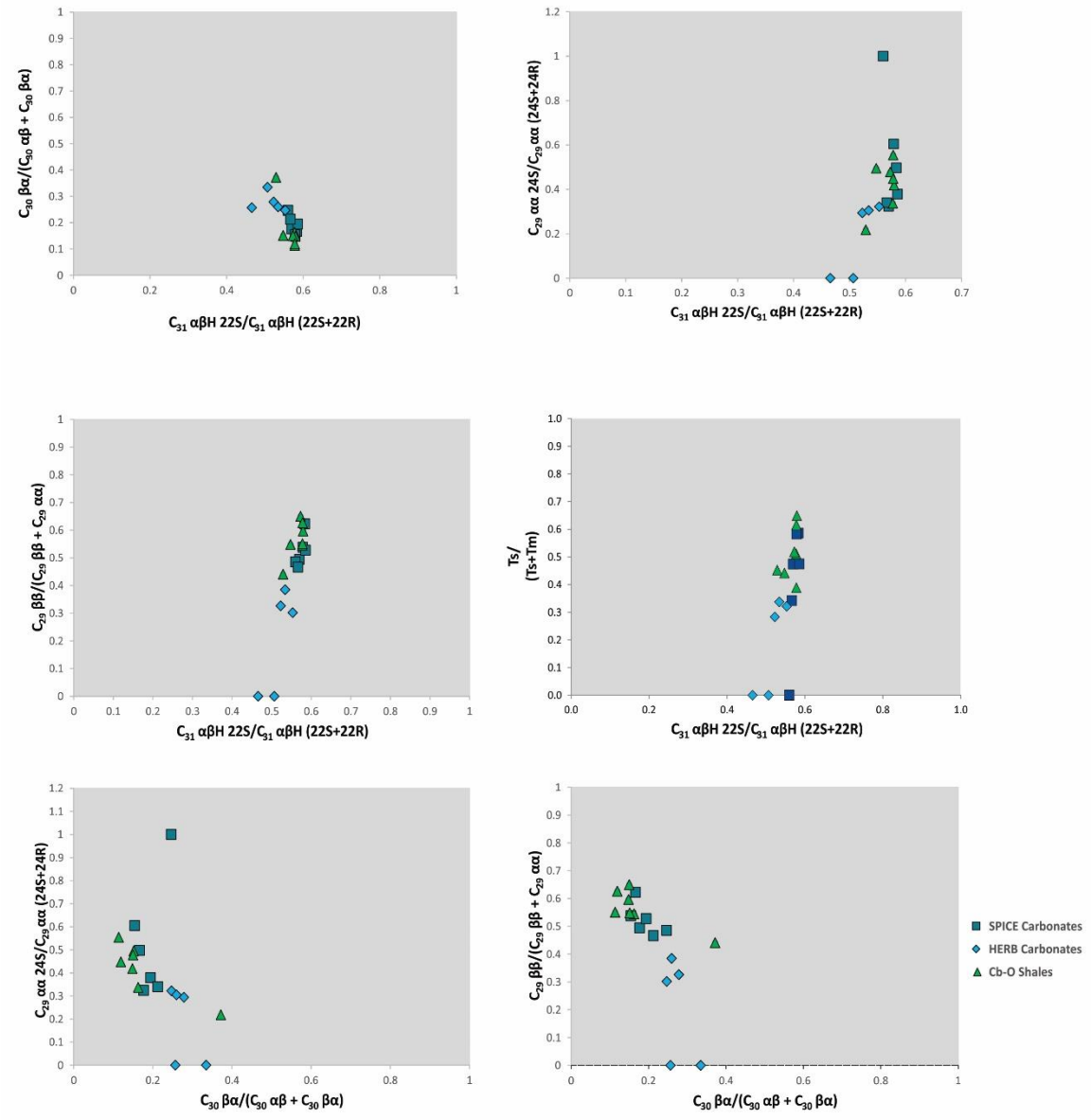


***Figure 13.*** *Cross-plots of various steroidal and hopanoid biomarkers to assess thermal maturation of the rock samples.*

### *3.3. Elemental Geochemistry*

Various trace elements have been detected and quantified from the rock samples that indicate paleoenvironment and redox changes during sediment deposition. The elements included from the analysis of ICP-MS are TOC%, Sr, Mo, U, V, As, Cr, Zn, Cu, Pb, Ni, Co, Fe, Mn, P, Ba, Th, Zr, Si, Ti, K, Al. There are published papers (Azmy et al., 2014, 2015; Azmy, 2019) regarding such trace elements in the same study area, therefore, the goal of using these published geochemical data is to assess if there is or is no correlation between these inorganic trace elements and the hydrocarbon biomarker ratios and indices determined by this study. For example, U, Th, V, Ni, Co, Cr can be used for determining redox conditions of the ancient depositional environment that can be statistically compared with Pristane/Phytane (Pr/Ph) ratio and gammacerane index (GI).

Concentrations of sedimentary organic matter in sedimentary rocks only record a fraction of the total productivity in the surface waters of the ocean. Sequestration of trace metals in sediments such as U, Th, V, Ni, Co, Cr can determine paleo-redox conditions in the depositional environment (Tribovillard et al., 2006). Novel biomarker and elemental ratios were both used to interpret the redox conditions within the sedimentary environment. Pr/Ph ratios indicated that sediment deposition in oxic to dysoxic water column containing anoxic sediments (Figure 7). Elemental paleo-redox proxies V/Ni and V/Cr similarly indicate oxic to anoxic water column during sediment deposition (Figure 15). Thorium to uranium ratio can also be used as paleo-redox proxy as Th is not highly affected by redox conditions. Sediments deposited from anoxic environments have high values of U and low Th/U (<2), whereas sediments of oxic environments have high Th/U (>2) and low U values (Azmy, 2019; Wignall and Twitchett, 1996). Most of the SPICE

and HERB Carbonates have low values of Th/U possibly suggesting uranium complexation to carbonate ions in the water column (Tribovillard et al., 2006; Klinkhammer and Palmer, 1991). On the other hand, most of the shale units have high Th/U that suggest oxic deposition.

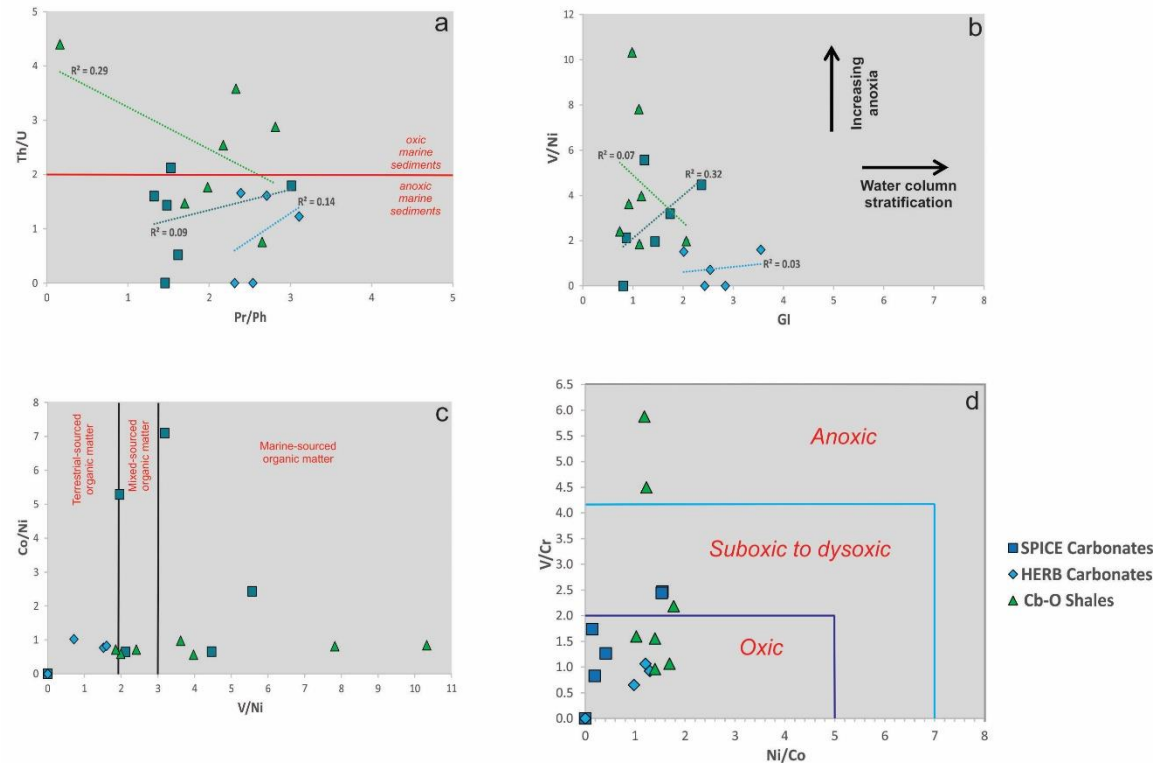


***Figure 14.*** *Cross-plots of (a) Pr/Ph versus Th/U, (b) GI versus V/Ni, (c) V/Ni versus Co/Ni (modified from Akinlua et al., 2016), (d) Ni/Co versus V/Cr (modified from Ventura and MacRae, 2019) derived from biomarker analyses and published trace element data (Azmy, 2019; Wang and Azmy 2019).*

Organic matter sources can be indicated using Co/Ni and V/Ni ratios. V/Ni values less than 1.9 indicate terrestrial-sourced organic matter, V/Ni values between 1.9 to 3 determine mixed-sourced from marine and terrestrial origin, while V/Ni values greater than 3 would indicate marine-sourced organic matter (Akinlua et al., 2016; Galarraga et al, 2008) (Figure 14c). The HERB carbonates mostly plot in the realm of terrestrial-sourced organic matter whereas SPICE carbonates and Cambro-Ordovician shales reside

in the mixed-sourced and marine-sourced organic matter, which agree with the results presented in Figure 8.

# 4. Summary: Biomarker and trace element ratios in a stratigraphic context

### *4.1.1. Geochemical trends along the SPICE event*

Selected source specific and thermal maturation biomarker parameters and paleoredox trace metal ratios are plotted in a stratigraphic context (Figure 15), which are also discussed in detail in sections 3.1, 3.2, and 3.3. There are notable geochemical trends at the base of Cambrian. One of the trend is the increase in Pr/Ph ratio from B14-2 (1.32) to B29-3 (3.01) and then decreases from B29-3 (3.01) to B31-9 (1.45), this may suggest the change of anoxic to oxic and then comes back down to anoxic conditions in the water column during the deposition of these carbonates that may be related to sea-level fluctuations. A change in sterane to hopane ratios in B29-3 increases going to B31-9 and decrease again from B31-9 to B36a-2, this suggest the difference in eukaryotic to prokaryotic inputs of organic matter. Gammacerane index (GI) increases from B1-1 (0.87) to B29-3 (2.36) and then decreases from B29-3 (2.36) to B31-9 (0.81) and increases from B31-9 (0.81) to B36c-1 (1.74). This trend can be considered to be changes in water column stratification. One of the SPICE carbonate samples (B29-3) did not show the appearance of 2α-methylhopanes (i.e., below detection limits) that shows sparse abundance of aerobic bacteria during deposition. In terms of its 3β-methylhopane counterparts, a decrease is shown from B1-1 to B29-3, increase from B29-3 to B31-9, and then decrease again from B31-9 to B36c-1. This suggests the absence and re-

appearance of methanotrophic bacteria in the depositional environment, as methanotrophs utilize methane as their energy source from methanogens. Methanogens only thrive in lacustrine conditions as such archaea get outcompeted by sulfate-reducing bacteria if the depositional system becomes rich in sulfate, hence, more marine conditions (Sela-Adler et al., 2017; Yoda et al., 1987). Thermal maturity parameters $C_{29}$ αα 24S and $C_{30}$ βα-moretane indicate early mature to mature source rocks of the samples. Th/U ratio shows low values (<2) for most of the carbonate units that indicate these were anoxic sediments during deposition. V/Ni, V/Cr, and Ni/Co ratios show shifts in values where it may suggest that the shifts corresponds to redox conditions.

### *4.1.2. Geochemical trends along the HERB event*

There are several notable trends based on biomarker ratios along the HERB event (Figure 15). There is a increase in Pr/Ph near the start of the HERB excursion and decrease in Pr/Ph ratio after the HERB event, suggesting changing oxygenation in the water column along with what gammecerane index is showing. There are drastic shifts in the sterane to hopane ratios in each sample that illustrate changes in eukaryotic to prokaryotic inputs of organic matter during sediment deposition. Only three samples showed presence of 2α-methylhopanes which may infer presence of oxygenic bacteria in such samples (MH1, MH5, MH23). Thermal maturity parameters demonstrate that the rock samples are early mature to mature, which are indicative of the possibility of generated petroleum. V/Ni, V/Cr, and Ni/Co show decreasing trend in three samples (MH1, MH3, MH5) that may suggest changes in redox conditions from dysoxic to oxic water column.

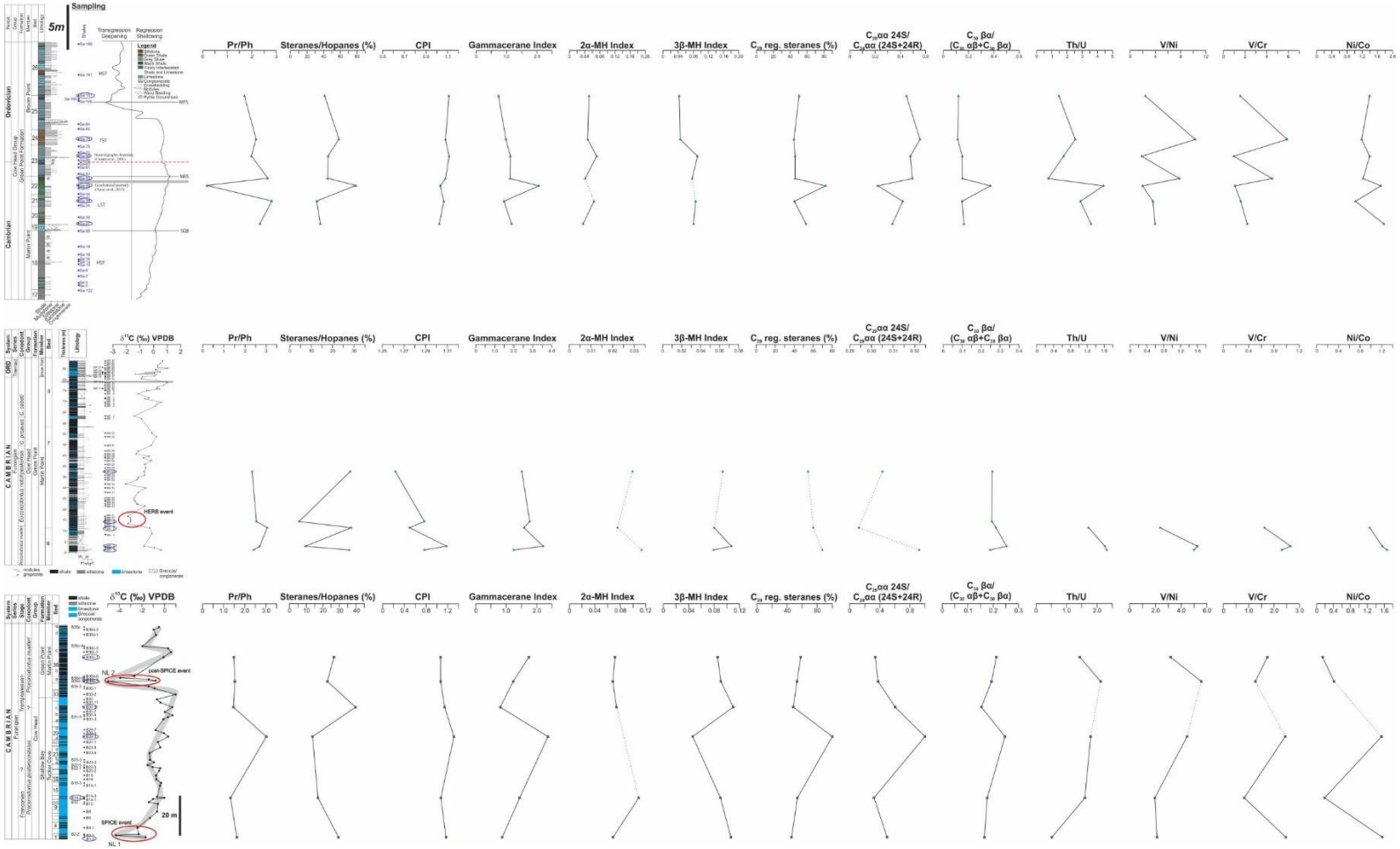


***Figure 15.*** *Various novel biomarker ratios and selected trace elements plotted in a stratigraphic context (modified from figures 2, 3, and 4) relating to different carbon isotope excursion events. The younging direction goes from bottom to top. Dashed lines represent that the some of the samples were lacking data for that specific parameters.*

### *4.1.3. Geochemical trends near Cambrian-Ordovician boundary*

A geochemical anomaly is observed near the Cambrian-Ordovician boundary (Figure 15) and along to where the geochemical anomaly is emplaced (between Sa-49 and Sa-53) based on trace element and carbon isotope study on Cambrian-Ordovician shales by Azmy et al. (2014; 2015). There is a sudden decrease of Pr/Ph value that indicate change from dysoxic to anoxic conditions. Increase in sterane/hopane is apparent near the anomaly which indicate increased proportion of eukaryotic to prokaryotic inputs of organic matter. Gammacerane index also has shown increasing value near the anomaly that determine increased water column stratification relative to other samples during deposition. Absence of 2α-methylhopanes and 3β-methylhopanes at the geochemical anomaly mentioned above can be interpreted that influence of oxygenic bacteria and methanotrophs were not present during sediment deposition. Thermal maturity parameters such as $C_{29}$ αα 24S and $C_{30}$ βα-moretane to $C_{30}$ αβ-hopane demonstrate early mature to mature source rocks of the shale units. Paleoredox trace metal ratios Th/U, V/Ni, V/Cr, Ni/Co show huge variations of values that may suggest changing redox conditions during deposition of siliciclastic sediments.

## 5. Conclusion

The slope-setting Cow Head carbonates and shales of the Cambrian-Ordovician GSSP boundary section in Martin Point, western Newfoundland, Canada exhibit a wide range of hydrocarbon biomarkers via solvent extraction and gas chromatographic techniques. Some of these compounds are *n*-Alkanes, acyclic isoprenoids, steranes, hopanes, tricyclic terpanes, and few aromatic hydrocarbons.

*n*-Alkanes and acyclic isoprenoids from the rock samples have documented the syngeneity of biomarkers, types of kerogen, and ancient depositional conditions. The source rocks are labelled as type II/III (oil and gas producing) and type III (gas producing) kerogen. Based on Pr/Ph ratios, the rocks were deposited within the range of dysoxic to oxic, possibly reaching anoxic conditions as well. Steroidal biomarkers have also been utilized for determining paleodepositional conditions. Based on $C_{27}$, $C_{28}$, and $C_{29}$ regular steranes, the depositional environment happened to be open marine environment that was enriched in plankton and algae.

Hopanoid biomarkers, which are commonly biosynthesized by prokaryotic organisms have been detected and used for determining the source of organic matter. Gammacerane, which originated from tetrahymanol, has been used to indicate water column stratification. Increased in water column stratification has been documented near the SPICE event, HERB event, and near the boundary. Presence of 2α-methylhopanes and 3β-methylhopanes have been used a proxy to determine nutrient loading and lacustrine conditions, respectively. These compounds have been detected in most of the Cow Head Group rock samples. The series of homohopanes was also detected that is used a proxy for examining the degree of anoxia in the depositional environment. Most of the samples have low abundance of homohopanes. Near the Cambrian-Ordovician boundary, there is an inverse relationship between decrease in Pr/Ph, increase in sterane/hopane ratios, and increase in gammacerane index that is suggesting oxygen drawdown near the boundary that also may have contributed to the redox conditions at depth.

Thermal maturation of the Cow Head Group was also assessed in this study. Hopane maturity parameters such as the ratio of moretane ($C_{30}$ βα) to hopane ($C_{30}$ αβ) (ave. 0.21), $C_{31}$ αβ-hopane 22S/$C_{31}$ αβ-hopane (22S+22R) (ave. 0.56), and the ratio of trisnorneohopane (Ts) and trisnorhopane (Tm) [Ts/(Ts + Tm)] (ave. 0.41) are showing that the Cow Head Group are early mature to mature source rocks. The sterane thermal maturity parameters such as $C_{29}$ ααS/$C_{29}$ αα(S+R) and $C_{29}$ ββ (S+R)/($C_{29}$ ββ (S+R) + $C_{29}$ αα(S+R)) agree with the results presented by the hopane maturity markers.

# 6. Appendix

***Table 1. Sample preparation measurements***

| *Sample ID* | *Stratigraphic Bed No.[1]* | *Lithology* | *Sediment wt. extracted (g)* | *Total Lipid Extract (g)* | *Polar fraction (mg)* | *Apolar fraction (mg)* |
|---|---|---|---|---|---|---|
| *B1-1* | 1 | Carbonate | 40.21 | 1.27545 | 2.77 | 26.76 |
| *B14-2* | 14 | Carbonate | 40.03 | 1.28988 | 3.97 | 5.38 |
| *B29-3* | 29 | Carbonate | 35.36 | 1.3402 | 1.12 | 4.68 |
| *B31-9* | 31 | Carbonate | 37.46 | 1.30559 | 6.38 | 2.6 |
| *B36a-2* | 36a | Carbonate | 40 | 1.31802 | 4.24 | 5.01 |
| *B36c-1* | 36c | Carbonate | 40.01 | 1.24518 | 30.82 | 42.98 |
| *MH1* | 6 | Carbonate | 40.04 | 1.26992 | 136.7 | 267.73 |
| *MH3* | 6 | Carbonate | 40.04 | 1.27552 | 3.35 | 19.16 |
| *MH5* | 7 | Carbonate | 30.03 | 1.30864 | 186.91 | 305.74 |
| *MH8* | 7 | Carbonate | 40.02 | 1.31884 | 2.33 | 1.46 |
| *MH23* | 7 | Carbonate | 40.01 | 1.31511 | 2.74 | 70.81 |
| *Sa-27* | 20 | Shale | 20.01 | 0.00791 | 7.05 | 0.86 |
| *Sa-39* | 21 | Shale | 20.01 | 0.00771 | 6.46 | 1.25 |
| *Sa-49* | 22 | Shale | 20.01 | 0.00794 | 7.62 | 0.32 |
| *Sa-53* | 23 | Shale | 14.46 | 0.01894 | 15 | 3.94 |
| *Sa-68* | 23 | Shale | 20.02 | 0.01517 | 13.01 | 2.16 |
| *Sa-79* | 24 | Shale | 20.04 | 0.0072 | 4.4 | 2.8 |
| *Sa-151* | 26 | Shale | 14.49 | 0.03079 | 23.18 | 7.61 |

***Table 2. n-Alkane FID concentrations***

| ***Sample ID*** | ***Stratigraphic Bed No.[1]*** | ***Lithology*** | ***n-$C_{12}$*** | ***n-$C_{13}$*** | ***n-$C_{14}$*** | ***n-$C_{15}$*** | ***n-$C_{16}$*** | ***n-$C_{17}$*** | ***n-$C_{18}$*** | ***n-$C_{19}$*** | ***n-$C_{20}$*** | ***n-$C_{21}$*** | ***n-$C_{22}$*** | ***n-$C_{23}$*** |
|---|---|---|---|---|---|---|---|---|---|---|---|---|---|---|
| *B1-1* | 1 | Carbonate | 0.01 | 0.01 | 0.08 | 0.94 | 3.40 | 8.24 | 5.98 | 10.04 | 4.44 | 4.85 | 3.37 | 3.34 |
| *B14-2* | 14 | Carbonate | 0.00 | 0.00 | 0.00 | 0.02 | 0.12 | 0.23 | 0.34 | 0.26 | 0.24 | 0.22 | 0.22 | 0.23 |
| *B29-3* | 29 | Carbonate | 0.00 | 0.00 | 0.00 | 0.01 | 0.01 | 0.02 | 0.02 | 0.02 | 0.02 | 0.02 | 0.03 | 0.03 |
| *B31-9* | 31 | Carbonate | 0.00 | 0.00 | 0.12 | 1.20 | 3.73 | 6.45 | 5.75 | 5.70 | 5.60 | 4.63 | 4.32 | 4.27 |
| *B36a-2* | 36a | Carbonate | 0.00 | 0.00 | 0.00 | 0.01 | 0.20 | 0.53 | 0.78 | 0.62 | 0.60 | 0.49 | 0.44 | 0.45 |
| *B36c-1* | 36c | Carbonate | 0.00 | 0.00 | 0.00 | 0.05 | 0.23 | 0.51 | 0.35 | 0.24 | 0.16 | 0.17 | 0.16 | 0.20 |
| *MH1* | 6 | Carbonate | 0.00 | 0.00 | 0.00 | 0.01 | 0.02 | 0.03 | 0.03 | 0.03 | 0.03 | 0.03 | 0.03 | 0.03 |
| *MH3* | 6 | Carbonate | 0.00 | 0.00 | 0.00 | 0.00 | 0.01 | 0.02 | 0.02 | 0.02 | 0.02 | 0.02 | 0.03 | 0.03 |
| *MH5* | 7 | Carbonate | 0.00 | 0.00 | 0.00 | 0.01 | 0.02 | 0.03 | 0.03 | 0.03 | 0.03 | 0.03 | 0.03 | 0.03 |
| *MH8* | 7 | Carbonate | 0.00 | 0.00 | 0.00 | 0.00 | 0.01 | 0.02 | 0.02 | 0.02 | 0.02 | 0.02 | 0.03 | 0.03 |
| *MH23* | 7 | Carbonate | 0.00 | 0.00 | 0.00 | 0.01 | 0.02 | 0.03 | 0.04 | 0.05 | 0.05 | 0.05 | 0.05 | 0.05 |
| *Sa27* | 20 | Shale | 0.07 | 0.22 | 0.15 | 0.56 | 2.01 | 2.74 | 2.71 | 2.45 | 2.05 | 1.78 | 1.49 | 1.55 |
| *Sa39* | 21 | Shale | 0.05 | 0.90 | 0.60 | 3.03 | 4.78 | 5.70 | 5.13 | 4.92 | 4.24 | 3.93 | 3.66 | 3.50 |
| *Sa49* | 22 | Shale | 0.20 | 3.92 | 0.42 | 16.21 | 0.63 | 0.40 | 0.62 | 0.38 | 0.52 | 0.64 | 0.86 | 1.58 |
| *Sa53* | 23 | Shale | 0.01 | 0.20 | 1.59 | 3.18 | 3.62 | 3.21 | 2.76 | 2.15 | 1.71 | 1.37 | 1.16 | 1.03 |
| *Sa68* | 23 | Shale | 0.00 | 0.03 | 0.69 | 2.09 | 3.23 | 3.28 | 2.67 | 2.57 | 2.55 | 2.87 | 2.89 | 3.13 |
| *Sa79* | 24 | Shale | 0.00 | 0.06 | 0.91 | 2.31 | 3.05 | 3.36 | 2.89 | 2.81 | 2.66 | 2.55 | 2.32 | 2.24 |
| *Sa151* | 26 | Shale | 0.14 | 1.43 | 3.44 | 3.91 | 3.59 | 3.18 | 2.61 | 2.34 | 1.94 | 1.76 | 1.48 | 1.38 |

| *Sample ID* | *n-$C_{24}$* | *n-$C_{25}$* | *n-$C_{26}$* | *n-$C_{27}$* | *n-$C_{28}$* | *n-$C_{29}$* | *n-$C_{30}$* | *n-$C_{31}$* | *n-$C_{32}$* | *n-$C_{33}$* | *n-$C_{34}$* | *n-$C_{35}$* | *n-$C_{36}$* |
|---|---|---|---|---|---|---|---|---|---|---|---|---|---|
| *B1-1* | 2.86 | 2.76 | 2.20 | 1.92 | 1.20 | 1.01 | 0.57 | 0.41 | 0.26 | 0.17 | 0.09 | 0.05 | 0.02 |
| *B14-2* | 0.26 | 0.28 | 0.27 | 0.25 | 0.20 | 0.18 | 0.13 | 0.10 | 0.06 | 0.04 | 0.02 | 0.02 | 0.01 |
| *B29-3* | 0.03 | 0.03 | 0.02 | 0.03 | 0.01 | 0.01 | 0.01 | 0.01 | 0.00 | 0.00 | 0.00 | 0.00 | 0.00 |
| *B31-9* | 3.95 | 4.38 | 3.63 | 3.15 | 2.22 | 1.85 | 1.23 | 0.97 | 0.61 | 0.49 | 0.32 | 0.27 | 0.15 |
| *B36a-2* | 0.44 | 0.44 | 0.40 | 0.35 | 0.25 | 0.19 | 0.13 | 0.09 | 0.05 | 0.03 | 0.02 | 0.01 | 0.01 |
| *B36c-1* | 0.24 | 0.30 | 0.31 | 0.32 | 0.28 | 0.25 | 0.20 | 0.15 | 0.10 | 0.07 | 0.04 | 0.02 | 0.01 |
| *MH1* | 0.03 | 0.03 | 0.02 | 0.03 | 0.02 | 0.02 | 0.01 | 0.01 | 0.00 | 0.00 | 0.00 | 0.00 | 0.00 |
| *MH3* | 0.03 | 0.03 | 0.02 | 0.02 | 0.01 | 0.01 | 0.01 | 0.01 | 0.01 | 0.00 | 0.00 | 0.00 | 0.00 |
| *MH5* | 0.03 | 0.03 | 0.02 | 0.03 | 0.01 | 0.02 | 0.01 | 0.01 | 0.01 | 0.00 | 0.00 | 0.00 | 0.00 |
| *MH8* | 0.02 | 0.03 | 0.02 | 0.02 | 0.01 | 0.01 | 0.00 | 0.00 | 0.00 | 0.00 | 0.00 | 0.00 | 0.00 |
| *MH23* | 0.05 | 0.05 | 0.04 | 0.04 | 0.02 | 0.02 | 0.01 | 0.01 | 0.01 | 0.00 | 0.00 | 0.00 | 0.00 |
| *Sa27* | 1.60 | 1.65 | 1.65 | 1.52 | 1.28 | 0.99 | 0.67 | 0.38 | 0.25 | 0.11 | 0.05 | 0.03 | 0.01 |
| *Sa39* | 3.46 | 3.56 | 3.38 | 2.95 | 2.41 | 2.01 | 1.44 | 1.08 | 0.56 | 0.31 | 0.15 | 0.11 | 0.06 |
| *Sa49* | 1.70 | 1.94 | 2.13 | 1.89 | 1.55 | 1.39 | 1.11 | 0.74 | 0.37 | 0.16 | 0.07 | 0.00 | 0.00 |
| *Sa53* | 0.87 | 0.77 | 0.64 | 0.55 | 0.43 | 0.39 | 0.27 | 0.21 | 0.14 | 0.08 | 0.05 | 0.04 | 0.03 |
| *Sa68* | 2.93 | 2.95 | 2.48 | 2.21 | 1.71 | 1.47 | 1.02 | 0.79 | 0.47 | 0.33 | 0.18 | 0.12 | 0.08 |
| *Sa79* | 2.07 | 1.89 | 1.52 | 1.19 | 0.95 | 0.75 | 0.55 | 0.45 | 0.28 | 0.20 | 0.09 | 0.08 | 0.04 |
| *Sa151* | 1.13 | 1.07 | 0.81 | 0.66 | 0.49 | 0.39 | 0.28 | 0.23 | 0.16 | 0.11 | 0.06 | 0.04 | 0.03 |

***Table 3. Acyclic isoprenoid FID concentrations***

| ***Sample ID*** | ***i-$C_{13}$*** | ***i-$C_{14}$*** | ***i-$C_{15}$*** | ***i-$C_{16}$*** | ***i-$C_{18}$*** | ***Pr*** | ***Ph*** |
|---|---|---|---|---|---|---|---|
| *B1-1* | 0.01 | 0.01 | 0.01 | 0.18 | 2.03 | 4.44 | 2.74 |
| *B14-2* | 0.00 | 0.00 | 0.00 | 0.01 | 0.13 | 0.24 | 0.18 |
| *B29-3* | 0.00 | 0.00 | 0.00 | 0.00 | 0.01 | 0.05 | 0.02 |
| *B31-9* | 0.00 | 0.00 | 0.01 | 0.46 | 4.38 | 5.28 | 3.62 |
| *B36a-2* | 0.00 | 0.00 | 0.00 | 0.00 | 0.24 | 0.45 | 0.30 |
| *B36c-1* | 0.00 | 0.00 | 0.00 | 0.01 | 0.23 | 0.38 | 0.26 |
| *MH1* | 0.00 | 0.01 | 0.00 | 0.01 | 0.01 | 0.06 | 0.02 |
| *MH3* | 0.00 | 0.00 | 0.00 | 0.00 | 0.01 | 0.04 | 0.01 |
| *MH5* | 0.00 | 0.00 | 0.00 | 0.01 | 0.01 | 0.07 | 0.02 |
| *MH8* | 0.00 | 0.00 | 0.00 | 0.00 | 0.01 | 0.04 | 0.01 |
| *MH23* | 0.00 | 0.00 | 0.00 | 0.00 | 0.02 | 0.08 | 0.03 |
| *Sa27* | 0.06 | 1.41 | 0.13 | 0.21 | 1.09 | 1.94 | 0.83 |
| *Sa39* | 0.04 | 1.00 | 0.16 | 0.99 | 2.55 | 3.65 | 1.30 |
| *Sa49* | 0.17 | 5.20 | 0.34 | 0.19 | 0.21 | 0.54 | 3.26 |
| *Sa53* | 0.00 | 0.07 | 0.18 | 1.05 | 1.56 | 1.65 | 0.62 |
| *Sa68* | 0.00 | 0.01 | 0.07 | 0.64 | 1.42 | 1.85 | 0.93 |
| *Sa79* | 0.00 | 0.00 | 0.13 | 0.93 | 2.13 | 3.29 | 1.51 |
| *Sa151* | 0.09 | 0.26 | 0.88 | 2.07 | 2.30 | 2.47 | 1.46 |

*Table 4. n-Alkane and acyclic isoprenoid parameters*

| *Sample ID* | *Pr/Ph* | *Pr/ n-$C_{17}$* | *Ph/ n-$C_{18}$* | *n-$C_{14}$/ (i-$C_{15}$ + n-$C_{14}$)* | *n-$C_{17}$/ (n-$C_{17}$+Pr)* | *n-$C_{18}$/ (n-$C_{18}$+Ph)* | *(n-$C_{23}$ to n-$C_{36}$)/ (n-$C_{12}$ to n-$C_{22}$)* | *(n-$C_{29}$ to n-$C_{31}$)/ ((n-$C_{17}$ to n-$C_{19}$)+(n-$C_{29}$ to n-$C_{31}$))* | *(Pr/n-$C_{17}$)/ (Ph/n-$C_{18}$))* | n-$C_{17}$/ (n-$C_{17}$+ n-$C_{27}$) |
|---|---|---|---|---|---|---|---|---|---|---|
| *B1-1* | 1.62 | 0.54 | 0.46 | 0.89 | 0.65 | 0.69 | 0.41 | 0.08 | 1.17 | 0.81 |
| *B14-2* | 1.32 | 1.04 | 0.53 | 0.85 | 0.49 | 0.65 | 1.24 | 0.33 | 1.95 | 0.48 |
| *B29-3* | 3.01 | 2.45 | 0.84 | 0.81 | 0.29 | 0.54 | 1.17 | 0.28 | 2.91 | 0.45 |
| *B31-9* | 1.46 | 0.82 | 0.63 | 0.92 | 0.55 | 0.61 | 0.73 | 0.18 | 1.30 | 0.67 |
| *B36a-2* | 1.53 | 0.85 | 0.38 | 0.82 | 0.54 | 0.73 | 0.78 | 0.18 | 2.26 | 0.60 |
| *B36c-1* | 1.48 | 0.74 | 0.74 | 0.87 | 0.57 | 0.57 | 1.34 | 0.36 | 1.00 | 0.62 |
| *MH1* | 2.39 | 1.96 | 0.79 | 0.62 | 0.34 | 0.56 | 0.99 | 0.30 | 2.48 | 0.53 |
| *MH3* | 2.71 | 2.65 | 0.89 | 0.61 | 0.27 | 0.53 | 1.17 | 0.29 | 3.00 | 0.42 |
| *MH5* | 3.11 | 2.60 | 0.79 | 0.74 | 0.28 | 0.56 | 1.02 | 0.29 | 3.30 | 0.50 |
| *MH8* | 2.54 | 2.39 | 0.87 | 0.76 | 0.30 | 0.54 | 1.02 | 0.25 | 2.75 | 0.49 |
| *MH23* | 2.31 | 2.18 | 0.75 | 0.86 | 0.31 | 0.57 | 0.94 | 0.23 | 2.92 | 0.49 |
| *Sa27* | 2.33 | 0.71 | 0.31 | 0.53 | 0.58 | 0.76 | 0.72 | 0.21 | 2.31 | 0.64 |
| *Sa39* | 2.81 | 0.64 | 0.25 | 0.79 | 0.61 | 0.80 | 0.68 | 0.22 | 2.53 | 0.66 |
| *Sa49* | 0.16 | 1.33 | 5.28 | 0.55 | 0.43 | 0.16 | 0.59 | 0.70 | 0.25 | 0.18 |
| *Sa53* | 2.65 | 0.51 | 0.23 | 0.90 | 0.66 | 0.82 | 0.26 | 0.10 | 2.28 | 0.85 |
| *Sa68* | 1.98 | 0.56 | 0.35 | 0.90 | 0.64 | 0.74 | 0.87 | 0.28 | 1.61 | 0.60 |
| *Sa79* | 2.17 | 0.98 | 0.52 | 0.87 | 0.50 | 0.66 | 0.54 | 0.16 | 1.87 | 0.74 |
| *Sa151* | 1.70 | 0.78 | 0.56 | 0.80 | 0.56 | 0.64 | 0.26 | 0.10 | 1.39 | 0.83 |

| | Carbon number preference indices | | | |
|---|---|---|---|---|
| ***Sample ID*** | CPI[2] ***0.5×((n-C25+n-C27+n-C29+ n-C31+n-C33)/ (n-C24+n-C26+n-C28+n-C30+ n-C32)+(n-C25+n-C27+n-C29+ n-C31+n-C33)/(n-C26+n-C28+n-C30+n-C32+ n-C34))*** | CPI(1) ***2×(n-C23+n-C25+n-C27+n-C29)/((n-C22+2× (n-C24+n-C26+n-C28)+n-C30)*** | OEP (1) ***(n-C21+6× n-C23+n-C25)/ (4×n-C22+ 4×n-C24)*** | OEP (2) ***(n-C25+6×n-C27+n-C29)/(4× n-C26+4× n-C28)*** |
| *B1-1* | 1.17 | 1.10 | 1.11 | 1.12 |
| *B14-2* | 1.07 | 1.03 | 0.98 | 1.04 |
| *B29-3* | 1.31 | 1.21 | 1.05 | 1.31 |
| *B31-9* | 1.14 | 1.09 | 1.05 | 1.07 |
| *B36a-2* | 1.07 | 1.03 | 1.02 | 1.05 |
| *B36c-1* | 1.07 | 1.06 | 1.04 | 1.04 |
| *MH1* | 1.29 | 1.22 | 1.06 | 1.32 |
| *MH3* | 1.31 | 1.24 | 1.07 | 1.38 |
| *MH5* | 1.28 | 1.20 | 1.05 | 1.34 |
| *MH8* | 1.29 | 1.24 | 1.13 | 1.27 |
| *MH23* | 1.26 | 1.17 | 1.06 | 1.26 |
| *Sa27* | 1.02 | 1.02 | 1.03 | 1.00 |
| *Sa39* | 1.06 | 1.02 | 1.00 | 1.01 |
| *Sa49* | 1.03 | 1.07 | 1.18 | 1.00 |
| *Sa53* | 1.08 | 1.03 | 1.02 | 1.05 |
| *Sa68* | 1.11 | 1.08 | 1.06 | 1.06 |
| *Sa79* | 1.08 | 1.02 | 1.02 | 0.99 |
| *Sa151* | 1.11 | 1.06 | 1.06 | 1.05 |

[1]Refer to Figures 2, 3, and 4.

[2]Carbon Preference Index = **0.5×((*n*-C25+*n*-C27+*n*-C29+*n*-C31+*n*-C33)/(*n*-C24+*n*-C26+*n*-C28+*n*-C30+*n*-C32)+(*n*-C25+*n*-C27+*n*-C29+*n*-C31+*n*-C33)/(*n*-C26+*n*-C28+*n*-C30+*n*-C32+*n*-C34));** CPI was measured using GC-MS by using extracted m/z 57 ion chromatogram by Bray and Evans, 1961.

***Table 5. Hydrocarbon biomarker source and thermal maturation parameters***

***Source specific biomarker ratios***

| | *Hopanes* | | | | *Tricyclic Terpanes* | *Gamma -cerane* | *Steranes* | | | | | |
|---|---|---|---|---|---|---|---|---|---|---|---|---|
| ***Sample ID*** | ***35/(31+32+33 +34+35) αβ (R+S)*** | ***29αβ/ 30αβ*** | ***BNH/ (BNH+ 30αβ)*** | ***C35αβ/ (C31αβ + C35αβ) (S+R)*** | ***(C21+C23 + C24)/(C1 9+ C20+C21 + C23+C24)*** | ***G×10/ (G+30α β)*** | ***Steranes / (steranes +hopane s) (%)*** | ***27/ (27+28+ 29) ααR steranes*** | ***28/ (27+28+ 29) ααR steranes*** | ***29/ (27+28+ 29) ααR steranes*** | ***29/ (27+28+ 29+30) ααR steranes (%)*** | ***29/ (27+30) ααR steranes*** |
| *B1-1* | 0.04 | 0.67 | 0.02 | 0.09 | 0.46 | 0.87 | 29.46 | 0.27 | 0.24 | 0.49 | 34.60 | 0.71 |
| *B14-2* | 0.04 | 0.81 | 0.01 | 0.09 | 0.45 | 1.44 | 17.05 | 0.13 | 0.14 | 0.73 | 38.35 | 0.71 |
| *B29-3* | 0.09 | 0.72 | - | 0.19 | 0.47 | 2.37 | 13.79 | - | - | - | - | - |
| *B31-9* | 0.05 | 0.40 | 0.04 | 0.10 | 0.44 | 0.81 | 39.62 | 0.26 | 0.27 | 0.47 | 34.97 | 0.78 |
| *B36a-2* | 0.06 | 0.84 | 0.10 | 0.15 | 0.40 | 1.23 | 22.70 | 0.25 | 0.10 | 0.65 | 38.74 | 0.70 |
| *B36c-1* | 0.05 | 0.92 | 0.12 | 0.10 | 0.61 | 1.74 | 26.66 | 0.15 | 0.07 | 0.78 | 47.10 | 0.96 |
| *MH1* | 0.00 | 0.65 | 0.15 | - | 0.39 | 2.01 | 27.68 | 0.05 | 0.00 | 0.95 | 52.46 | 1.10 |
| *MH3* | 0.08 | 0.70 | 0.14 | 0.18 | - | 3.55 | 7.20 | - | - | - | - | - |
| *MH5* | 0.05 | 0.64 | 0.11 | 0.11 | 0.56 | 2.54 | 28.69 | 0.10 | 0.09 | 0.82 | 45.71 | 0.92 |
| *MH8* | 0.00 | 0.66 | 0.13 | - | - | 2.84 | 4.31 | - | - | - | - | - |
| *MH23* | 0.06 | 0.66 | 0.12 | 0.12 | 0.47 | 2.43 | 28.19 | 0.10 | 0.11 | 0.80 | 44.05 | 0.88 |
| *Sa27* | 0.02 | 0.73 | 0.03 | 0.05 | 0.42 | 1.17 | 35.89 | 0.18 | 0.10 | 0.72 | 44.07 | 0.88 |
| *Sa39* | 0.03 | 0.64 | 0.02 | 0.06 | 0.46 | 0.92 | 31.80 | 0.29 | 0.29 | 0.42 | 31.25 | 0.66 |
| *Sa49* | 0.00 | 0.75 | 0.04 | - | - | 2.06 | 78.77 | 0.03 | 0.03 | 0.95 | 54.32 | 1.23 |
| *Sa53* | 0.04 | 0.73 | 0.07 | 0.07 | 0.49 | 1.12 | 44.89 | 0.30 | 0.22 | 0.48 | 33.44 | 0.66 |
| *Sa68* | 0.05 | 0.52 | 0.02 | 0.11 | 0.55 | 1.13 | 45.48 | 0.27 | 0.37 | 0.36 | 28.56 | 0.67 |
| *Sa79* | 0.04 | 0.57 | 0.03 | 0.08 | 0.46 | 0.98 | 58.43 | 0.28 | 0.36 | 0.36 | 27.86 | 0.62 |

| | | | | | | | | | | | | |
|---|---|---|---|---|---|---|---|---|---|---|---|---|
| *Sa151* | 0.04 | 0.76 | 0.02 | 0.09 | 0.58 | 0.74 | 41.27 | 0.23 | 0.29 | 0.48 | 33.51 | 0.72 |

## *Source specific biomarker ratios (continued)*

| *Sample ID* | *27/ (27+28+29) ααR+ααS+ββS steranes* | *28/ (27+28+29) ααR+ααS+ββS steranes* | *29/ (27+28+29) ααR+ααS+ββS steranes* | *27/ (27+28+29) αα+ββ (S+R) (%)* | *28/ (27+28+29) αα+ββ (S+R) (%)* | *29/ (27+28+29) αα+ββ (S+R) (%)* | *2α-MHI* | *3β-MHI* | *(DBT+all M- & DMDBTs)/ (P+all M- ,DM-, & ET-Ps)* |
|---|---|---|---|---|---|---|---|---|---|
| *B1-1* | 0.23 | 0.30 | 0.48 | 17.95 | 36.17 | 45.88 | 0.069 | 0.107 | 0.29 |
| *B14-2* | 0.16 | 0.28 | 0.56 | 12.94 | 33.24 | 53.82 | 0.109 | 0.090 | 0.25 |
| *B29-3* | 0.00 | 0.00 | 1.00 | - | - | 100.00 | | 0.046 | 0.75 |
| *B31-9* | 0.21 | 0.28 | 0.51 | 16.29 | 35.52 | 48.19 | 0.074 | 0.110 | 0.12 |
| *B36a-2* | 0.22 | 0.22 | 0.56 | 17.77 | 29.04 | 53.19 | 0.068 | 0.091 | 0.20 |
| *B36c-1* | 0.20 | 0.20 | 0.61 | 16.10 | 25.83 | 58.07 | 0.072 | 0.086 | 0.14 |
| *MH1* | 0.08 | 0.22 | 0.71 | 6.62 | 23.83 | 69.56 | 0.033 | 0.054 | - |
| *MH3* | - | - | - | - | - | - | - | 0.072 | - |
| *MH5* | 0.11 | 0.25 | 0.64 | 8.86 | 31.10 | 60.04 | 0.022 | 0.054 | - |
| *MH8* | - | - | - | - | - | - | - | 0.000 | - |
| *MH23* | 0.14 | 0.30 | 0.56 | 11.29 | 34.18 | 54.53 | 0.029 | 0.063 | - |
| *Sa-27* | 0.23 | 0.20 | 0.57 | 18.71 | 22.46 | 58.83 | 0.036 | 0.081 | 0.08 |
| *Sa-39* | 0.30 | 0.26 | 0.44 | 24.57 | 30.43 | 45.00 | 0.064 | 0.086 | 0.07 |
| *Sa-49* | 0.07 | 0.06 | 0.87 | 5.49 | 12.45 | 82.06 | - | - | 0.20 |
| *Sa-53* | 0.30 | 0.27 | 0.43 | 24.99 | 29.19 | 45.83 | 0.041 | 0.077 | 0.12 |
| *Sa-68* | 0.23 | 0.34 | 0.43 | 19.12 | 34.99 | 45.89 | 0.072 | 0.091 | 0.06 |
| *Sa-79* | 0.29 | 0.34 | 0.37 | 21.66 | 33.87 | 44.47 | 0.048 | 0.046 | 0.06 |
| *Sa-151* | 0.23 | 0.28 | 0.49 | 17.87 | 31.49 | 50.64 | 0.051 | 0.043 | 0.22 |

***Thermal maturation biomarker ratios***

| | Hopanes | | | | | Steranes | |
|---|---|---|---|---|---|---|---|
| ***Sample ID*** | ***Ts/ (Ts+Tm)*** | ***31αβ 22S/ 31αβ(S+R)*** | ***32αβ 22S/ 32αβ(S+R)*** | ***30βα/ (30αβ+30βα)*** | ***31αβ(S+R)/ (29αβ+30αβ)*** | ***29ααS/ 29αα(S+R)*** | ***29ββ/ (29ββ+29αα)*** |
| *B1-1* | 0.59 | 0.58 | 0.60 | 0.17 | 0.38 | 0.50 | 0.62 |
| *B14-2* | 0.47 | 0.57 | 0.57 | 0.18 | 0.48 | 0.32 | 0.49 |
| *B29-3* | | 0.56 | 0.54 | 0.25 | 0.49 | 1.00 | 0.48 |
| *B31-9* | 0.58 | 0.58 | 0.57 | 0.15 | 0.47 | 0.60 | 0.54 |
| *B36a-2* | 0.48 | 0.59 | 0.56 | 0.19 | 0.40 | 0.38 | 0.53 |
| *B36c-1* | 0.34 | 0.57 | 0.57 | 0.21 | 0.49 | 0.34 | 0.47 |
| *MH1* | 0.32 | 0.55 | 0.52 | 0.25 | 0.47 | 0.32 | 0.30 |
| *MH3* | 0.00 | 0.51 | 0.53 | 0.33 | 0.93 | - | - |
| *MH5* | 0.28 | 0.52 | 0.54 | 0.28 | 0.57 | 0.29 | 0.33 |
| *MH8* | 0.00 | 0.47 | 0.57 | 0.26 | 0.68 | - | - |
| *MH23* | 0.34 | 0.53 | 0.54 | 0.26 | 0.59 | 0.31 | 0.38 |
| *Sa-27* | 0.51 | 0.58 | 0.55 | 0.16 | 0.37 | 0.34 | 0.55 |
| *Sa-39* | 0.65 | 0.58 | 0.56 | 0.15 | 0.42 | 0.42 | 0.60 |
| *Sa-49* | 0.45 | 0.53 | 0.58 | 0.37 | 0.42 | 0.22 | 0.44 |
| *Sa-53* | 0.44 | 0.55 | 0.55 | 0.15 | 0.39 | 0.50 | 0.55 |
| *Sa-68* | 0.52 | 0.57 | 0.56 | 0.15 | 0.52 | 0.48 | 0.65 |
| *Sa-79* | 0.62 | 0.58 | 0.57 | 0.11 | 0.48 | 0.55 | 0.55 |
| *Sa-151* | 0.39 | 0.58 | 0.55 | 0.12 | 0.34 | 0.45 | 0.63 |

*Table 6. Trace element ratios[1,2] (in ppm)*

| *Sample ID* | *V* | *Ni* | *Co* | *Cr* | *Th* | *U* | *Th/U* | *V/Ni* | *V/Cr* | *Ni/Co* | *Co/Ni* |
|---|---|---|---|---|---|---|---|---|---|---|---|
| *B1-1* | 2.85 | 1.34 | 0.87 | 1.16 | 0.93 | 1.79 | 0.52 | 2.12 | 2.47 | 1.55 | 0.65 |
| *B14-2* | 1.37 | 0.70 | 3.68 | 1.65 | 0.43 | 0.27 | 1.60 | 1.96 | 0.83 | 0.19 | 5.29 |
| *B29-3* | 6.57 | 1.47 | 0.96 | 2.69 | 0.69 | 0.38 | 1.79 | 4.46 | 2.44 | 1.54 | 0.65 |
| *B31-9* | - | - | - | - | - | - | - | - | - | - | - |
| *B36a-2* | 1.92 | 0.34 | 0.84 | 1.52 | 0.39 | 0.18 | 2.12 | 5.57 | 1.26 | 0.41 | 2.43 |
| *B36c-1* | 2.46 | 0.77 | 5.48 | 1.42 | 0.59 | 0.41 | 1.43 | 3.19 | 1.74 | 0.14 | 7.10 |
| *MH1* | 4.65 | 3.07 | 2.37 | 5.04 | 0.58 | 0.35 | 1.66 | 1.52 | 0.92 | 1.30 | 0.77 |
| *MH3* | 5.81 | 3.62 | 3.00 | 5.46 | 0.66 | 0.41 | 1.61 | 1.60 | 1.06 | 1.21 | 0.83 |
| *MH5* | 2.93 | 4.10 | 4.20 | 4.50 | 0.24 | 0.19 | 1.23 | 0.71 | 0.65 | 0.98 | 1.02 |
| *MH8* | - | - | - | - | - | - | - | - | - | - | - |
| *MH23* | - | - | - | - | - | - | - | - | - | - | - |
| *Sa-27* | 194.70 | 49.00 | 27.67 | 89.03 | 10.01 | 2.79 | 3.58 | 3.97 | 2.19 | 1.77 | 0.56 |
| *Sa-39* | 107.32 | 29.64 | 28.95 | 67.23 | 6.94 | 2.41 | 2.88 | 3.62 | 1.60 | 1.02 | 0.98 |
| *Sa-49* | 63.56 | 31.97 | 18.93 | 59.51 | 6.38 | 1.45 | 4.40 | 1.99 | 1.07 | 1.69 | 0.59 |
| *Sa-53* | 305.03 | 39.01 | 31.84 | 67.82 | 7.40 | 9.74 | 0.76 | 7.82 | 4.50 | 1.23 | 0.82 |
| *Sa-68* | 56.76 | 30.67 | 21.94 | 59.04 | 4.79 | 2.71 | 1.77 | 1.85 | 0.96 | 1.40 | 0.72 |
| *Sa-79* | 288.41 | 27.93 | 23.57 | 49.07 | 6.45 | 2.54 | 2.54 | 10.33 | 5.88 | 1.19 | 0.84 |
| *Sa-151* | 77.86 | 32.27 | 23.10 | 50.02 | 4.85 | 3.30 | 1.47 | 2.41 | 1.56 | 1.40 | 0.72 |

[1]Azmy (2019; 2019)

[2]Wang and Azmy (2019)

*Table 7. List of abbreviation for organic compounds*

| Abbreviation | Compound |
|---|---|
| Sat | saturate fraction |
| Aro | aromatic fraction |
| *i*-$C_9$ | iso-nonane |
| *n*-$C_9$ | normal-nonane |
| *i*-$C_{10}$ | iso-decane |
| *n*-$C_{10}$ | normal-decane |
| *i*-$C_{11}$ | iso-undecane |
| *n*-$C_{11}$ | normal-undecane |
| *n*-$C_{12}$ | normal-dodecane |
| *i*-$C_{13}$ | iso-tridecane |
| *i*-$C_{14}$ | iso-tetradecane |
| *n*-$C_{13}$ | normal-tridecane |
| *i*-$C_{15}$ | iso-pentadecane |
| *n*-$C_{14}$ | normal-tetradecane |
| *i*-$C_{16}$ | iso-hexadecane |
| *n*-$C_{15}$ | normal-pentadecane |
| *n*-$C_{16}$ | normal-hexadecane |
| *i*-$C_{18}$ | iso-octadecane |
| *n*-$C_{17}$ | normal-heptadecane |
| Pr | pristane (iso-nonadecane) |
| *n*-$C_{18}$ | normal-octadecane |
| Ph | phytane (iso-eicosane) |
| *n*-$C_{19}$ | normal-nonadecane |
| *n*-$C_{20}$ | normal-eicosane |
| *n*-$C_{21}$ | normal-heneicosane |

| Abbreviation | Compound |
|---|---|
| 34αβR | 17α, 21β, 22(R)-tetrakishomohopane |
| 35αβS | 17α, 21β, 22(S)-pentakishomohopane |
| 35αβR | 17α, 21β, 22(R)-pentakishomohopane |
| 21αα | C21-5α, 14α, 17α-pregnane |
| 21ββ | C21-5α, 14β, 17β-pregnane |
| 22αα | C22-5α, 14α, 17α-pregnane |
| 22ββ | C22-5α, 14β, 17β-pregnane |
| 27dβS | 13β, 17α, 20(S)-cholestane |
| 27dβR | 13β, 17α, 20(R)-cholestane |
| 27dαR | 13α, 17β, 20(R)-cholestane |
| 27dαS | 13α, 17β, 20(S)-cholestane |
| 28dβS#1 | 24-methyl-13β, 17α, 20(S)-cholestane #1 |
| 28dβS#2 | 24-methyl-13β, 17α, 20(S)-cholestane #2 |
| 28dβR#1 | 24-methyl-13β, 17α, 20(R)-cholestane #1 |
| 28dβR#2 | 24-methyl-13β, 17α, 20(R)-cholestane #2 |
| 28dαR | 24-methyl-13α, 17β, 20(R)-cholestane |
| 27ααS | 5α, 14α, 17α, 20(S)-cholestane |
| 27ββR+29dβS | 5α, 14β, 17β, 20(R)-cholestane + 24-ethyl-13β, 17α, 20(S)-cholestane |
| 27ββS | 5α, 14β, 17β, 20(S)-cholestane |
| 28dαS | 24-methyl-13α, 17β, 20(S)-cholestane |
| 27ααR | 5α, 14α, 17α, 20(R)-cholestane |
| 29dβR | 24-ethyl-13β, 17α, 20(R)-cholestane |
| 29dαR | 24-ethyl-13α, 17β, 20(R)-cholestane |
| 28ααS | 24-methyl-5α, 14α, 17α, 20(S)-cholestane |
| 29dαS | 24-ethyl-13α, 17β, 20(S)-cholestane |

| Abbreviation | Compound |
|---|---|
| *n*-$C_{22}$ | normal-docosane |
| *n*-$C_{23}$ | normal-tricosane |
| *n*-$C_{24}$ | normal-tetracosane |
| *n*-$C_{25}$ | normal-pentacosane |
| *n*-$C_{26}$ | normal-hexacosane |
| *n*-$C_{27}$ | normal-heptacosane |
| *n*-$C_{28}$ | normal-octacosane |
| *n*-$C_{29}$ | normal-nonacosane |
| *n*-$C_{30}$ | normal-triacontane |
| *n*-$C_{31}$ | normal-hentriacontane |
| *n*-$C_{32}$ | normal-dotriacontane |
| *n*-$C_{33}$ | normal-tritriacontane |
| *n*-$C_{34}$ | normal-tetratriacontane |
| *n*-$C_{35}$ | normal-pentatriacontane |
| *n*-$C_{36}$ | normal-hexatriacontane |
| 25nor28αβ | 17α, 21β-25,28,30-trisnorhopane |
| 25nor29αβ | 17α, 21β-25,30-bisnorhopane |
| 25nor30αβ | 17α, 21β-25-norhopane |
| 25nor31αβ | 17α, 21β, 22(R/S)-25-norhomohopane |
| 19C | C19H34 tricyclic terpane |
| IP | isopimarane |
| 20C | C20H36 tricyclic terpane |
| 21C | C21H38 tricyclic terpane |
| 23C | C23H42 tricyclic terpane |
| 24C | C24H44 tricyclic terpane |
| 26C | C26H48 tricyclic terpane |
| 28C | C28H52 tricyclic terpane |

| Abbreviation | Compound |
|---|---|
| 28βββR | 24-methyl-5α, 14β, 17β, 20(R)-cholestane |
| 28βββS | 24-methyl-5α, 14β, 17β, 20(S)-cholestane |
| 28αααR | 24-methyl-5α, 14α, 17α, 20(R)-cholestane |
| 29αααS | 24-ethyl-5α, 14α, 17α, 20(S)-cholestane |
| 29βββR | 24-ethyl-5α, 14β, 17β, 20(R)-cholestane |
| 29βββS | 24-ethyl-5α, 14β, 17β, 20(S)-cholestane |
| 29αααR | 24-ethyl-5α, 14α, 17α, 20(R)-cholestane |
| 30βββS | 24-propyl-5α, 14β, 17β, 20(S)-cholestane |
| 30αααR | 24-propyl-5α, 14α, 17α, 20(R)-cholestane |
| 27βββR | 5α, 14β, 17β, 20(R)-cholestane |
| 27βββS | 5α, 14β, 17β, 20(S)-cholestane |
| 28βββR | 24-methyl-5α, 14β, 17β, 20(R)-cholestane |
| 28βββS | 24-methyl-5α, 14β, 17β, 20(S)-cholestane |
| 29βββR | 24-ethyl-5α, 14β, 17β, 20(R)-cholestane |
| 29βββS | 24-ethyl-5α, 14β, 17β, 20(S)-cholestane |
| 30βββR | 24-propyl-5α, 14β, 17β, 20(R)-cholestane |
| 30βββS | 24-propyl-5α, 14β, 17β, 20(S)-cholestane |
| 27dβS | 13β, 17α, 20(S)-cholestane |
| 27dβR | 13β, 17α, 20(R)-cholestane |
| 27dαR | 13α, 17β, 20(R)-cholestane |
| 27dαS | 13α, 17β, 20(S)-cholestane |
| 28dβS#1 | 24-methyl-13β, 17α, 20(S)-cholestane #1 |
| 28dβS#2 | 24-methyl-13β, 17α, 20(S)-cholestane #2 |
| 28dβR#1 | 24-methyl-13β, 17α, 20(R)-cholestane #1 |
| 28dβR#2 | 24-methyl-13β, 17α, 20(R)-cholestane #2 |
| 28dαR | 24-methyl-13α, 17β, 20(R)-cholestane |
| 29dβS | 24-ethyl-13β, 17α, 20(S)-cholestane |

| Abbreviation | Compound |
|---|---|
| 29C | C29H54 tricyclic terpane |
| Ts | 18α-22,29,30-trisnorneohopane |
| A | unknown pentacyclic triterpenoid |
| Tm | 17α-22,29,30-trisnorhopane |
| 30C | C30H56 tricyclic terpane |
| BNH | 17α, 21β-28,30-bisnorhopane |
| 25-norH | 17α, 21β-25-norhopane |
| 29αβ | 17α, 21β-30-norhopane |
| 29Ts | 18α-30-norneohopane |
| 30d | 15α-methyl-17α-27-norhopane |
| 29βα | 17β, 21α-30-norhopane |
| 30αβ | 17α, 21β-hopane |
| 30βα | 17β, 21α-hopane (moretane) |
| 31αβS | 17α, 21β, 22(S)-homohopane |
| 31αβR | 17α, 21β, 22(R)-homohopane |
| G | gammacerane |
| 31βα | 17β, 21α-homohopane |
| 32αβS | 17α, 21β, 22(S)-bishomohopane |
| 32αβR | 17α, 21β, 22(R)-bishomohopane |
| 33αβS | 17α, 21β, 22(S)-trishomohopane |
| 33αβR | 17α, 21β, 22(R)-trishomohopane |
| 34αβS | 17α, 21β, 22(S)-tetrakishomohopane |
| MDBT | methyldibenzothiophene |
| 1MDBT | 1-methyldibenzothiophenes |
| 4MDBT | 4-methyldibenzothiophenes |
| DMDBTs | dimethyldibenzothiophenes |

| Abbreviation | Compound |
|---|---|
| 28dαS | 24-methyl-13α, 17β, 20(S)-cholestane |
| 29dβR | 24-ethyl-13β, 17α, 20(R)-cholestane |
| 29dαR | 24-ethyl-13α, 17β, 20(R)-cholestane |
| 29dαS | 24-ethyl-13α, 17β, 20(S)-cholestane |
| 1MN | 1-methylnaphthalenes |
| 2MN | 2-methylnaphthalenes |
| 1,5DMN | 1,5-dimethylnaphthalenes |
| 2,6DMN | 2,6-dimethylnaphthalenes |
| 2,7DMN | 2,7-dimethylnaphthalenes |
| EN | ethylnaphthalene |
| 1,3,7TMN | 1,3,7-trimethylnaphthalenes |
| 1,2,5TMN | 1,2,5-trimethylnaphthalenes |
| 2,3,6TMN | 2,3,6-trimethylnaphthalenes |
| 1,3,5TMN | 1,3,5-trimethylnaphthalenes |
| 1,4,6TMN | 1,4,6-trimethylnaphthalenes |
| 1,3,7TMN | 1,3,7-trimethylnaphthalenes |
| 1,3,6TMN | 1,3,6-trimethylnaphthalenes |
| P | phenanthrene |
| Ps | phenanthrene and anthracene |
| 1MP | 1-methylphenanthrenes |
| 2MP | 2-methylphenanthrenes |
| 3MP | 3-methylphenanthrenes |
| 9MP | 9-methylphenanthrenes |
| DMP | dimethylphenanthrenes |
| EP | ethylphenanthrene |
| DBT | dibenzothiophene |

***List of selected formula and references:***

[1]$C_{27}$, $C_{28,}$ $C_{29}$ S/(S+R) = 5α(H),14α(H),17α(H)-sterane-20S/(5α(H),14α(H),17α(H)-sterane-20S+5α(H),14α(H),17α(H)-sterane-20R for $C_{27}$, $C_{28,}$ and $C_{29}$, respectively (Seifert and Moldowan, 1986).

[2]$C_{27}$ ββ/(αα+ββ) = $C_{27}$ 5α(H),14β(H),17β(H)-cholestane 20(S+R)/[ $C_{27}$ 5α(H),14β(H),17β(H)-cholestane 20(S+R) + 5α(H),14α(H),17α(H)-cholestane 20(S+R)], $C_{28}$ ββ/(αα+ββ) and $C_{29}$ ββ/(αα+ββ) is calculated from the same equation as $C_{27}$ ββ/(αα+ββ (Seifert and Moldowan, 1986).

[3]$C_{28}/(C_{28}+C_{29})$ = [∑$C_{28}$ 13β(H),17α(H)-diasterane-20(S+R) + 5α(H),14α(H),17α(H)-cholestane 20(S+R) + 5α(H),14β(H),17β(H)-cholestane-20(S+R)]/[∑$C_{28}$ + $C_{29}$ 13β(H),17α(H)-diasterane-20(S+R) + 5α(H),14α(H),17α(H)-cholestane 20(S+R) + 5α(H),14β(H),17β(H)-cholestane-20(S+R)] (Grantham and Wakefield, 1988).

[4]Reg$C_{27}$ (%) = [$C_{27}$ 5α(H),14α(H),17α(H)-cholestane 20(S+R) + ($C_{27}$ 5α(H),14β(H),17β(H)-cholestane-20(S+R))]/[∑$C_{27}$ to $C_{29}$ (5α(H),14β(H),17β(H)-steranes 20(S+R) + 5α(H),14α(H),17α(H)-steranes 20(S+R))]; Reg$C_{28}$ (%) and Reg$C_{29}$ (%) are calculated from the same equation as Reg$C_{27}$ (%).

[5]$C_{27}/C_{29}$ = (Ts +Tm)/$C_{29}$ 17α(H),21β(H)-hopane; $C_{29}/C_{30}$ = $C_{29}$ 17α(H),21β(H)-hopane / $C_{30}$ 17α(H),21β(H)-hopane;
$C_{30}/C_{31}$ = $C_{30}$ 17α(H),21β(H)-hopane / $C_{31}$ 17α(H),21β(H)-hopane 22(S+R).

[6]Ts and Tm = $C_{27}$ 17α(H)-22,29,30-trisnorhopane and 18α(H)-22,29,30-trisnorhopane, respectively.

[7]$C_{29}$Ts/$C_{29}$H = $C_{29}$ 17α(H)-22,29,30-trisnorhopane / $C_{29}$ 17α(H),21β(H)-hopane.

[8]$C_{31}$S/(S+R) = $C_{31}$ 17α(H),21β(H)-hopane 22S / $C_{31}$ 17α(H),21β(H)-hopane 22(S+R).

[9]$C_{30}$Mor/$C_{30}$Hop = $C_{30}$ 17β(H),21α(H)-hopane/$C_{30}$ 17α(H),21β(H)-hopane.

[10]Gammacerane Index (GI) = Gammacerane/(Gammacerane + $C_{30}$ 17α(H),21β(H)-hopane) (Moldowan *et al*., 1985).

[11]$C_{31}$ 2α-Methylhopane Index ($C_{31}$ 2α-MHI) = $C_{31}$-2α-methylhopane / ($C_{31}$-2α-methylhopane + $C_{30}$ 17α(H),21β(H)-hopane) (Summons *et al*., 1999).

[12]H/S = [∑ $C_{27}$ 17α(H)-22,29,30-trisnorhopane + $C_{27}$ 18α(H)-22,29,30-trisnorhopane + $C_{29}$ 17α(H)-22,29,30-trisnorhopane + $C_{29}$-$C_{30}$ 17α(H),21β(H)-hopane + $C_{31}$-$C_{35}$17α(H),21β(H)-hopane 22(S+R) + $C_{31}$ 2α(H)-methylhopane] / (∑ $C_{27}$-$C_{29}$ 5α(H),14α(H),17α(H) and 5α(H),14β(H),17β(H)-steranes and 13β(H),17α(H)-diasteranes).

## 7. List of References


Akinlua, A., Olise, F. S., Akomolafe, A. O., and McCrindle, R. I. (2016). Rare earth element geochemistry of petroleum source rocks from northwestern Niger Delta. *Marine and Petroleum Geology, 77*, 409-417.

Azmy, K., Kendall, B., Brand, U., Stouge, S., Gordon, G. W. (2015). Redox conditions across the Cambrian-Ordovician boundary: Elemental and isotopic signatures retained in the GSSP carbonates. *Palaeogeography, Palaeoclimatology, Palaeoecology, 440*, 440-454.

Azmy, K., Stouge, S., Brand, U., Bagnoli, G., and Ripperdan, R. (2014). High-resolution chemostratigraphy of the Cambrian-Ordovician GSSP: Enhanced global correlation tool. *Palaeogeography, Palaeoclimatology, Palaeoecology, 409*, 135-144.

Azmy, K. (2019). Carbon-isotope stratigraphy of the SPICE event (Upper Cambrian) in eastern Laurentia: implications for global correlation and a potential reference section. *Geological Magazine, 156*, 1311-1322.

Azmy, K. (2019). Carbon-isotope stratigraphy of the uppermost Cambrian in eastern Laurentia: implications for global correlation. *Geological Magazine, 156*, 759-771.

Baskin, D. K. (1997). Atomic H/C Ratio of Kerogen as an Estimate of Thermal Maturity and Organic Matter Conversion. *The American Association of Petroleum Geologists, 81*, 1437-1450.

Bertrand, R., Lavoie, D., and Fowler, M. (2003). Cambrian-Ordovician shales in the Humber Zone: thermal maturation and source rock potential. *Bulletin of Canadian Petroleum Geology, 51*, 213-233.

Bisnaire, A. C., Azmy, K., Kendall, B., and Stouge, S. (n.d.). Trace element variations in the shales across the Cambrian-Ordovician boundary: implications for environmental changes associated with sea-level variations. *To be published in "Sedimentology".*

Bray, E.E., Evans, E.D., 1961. Distribution of n-paraffin hydrocarbons in nature. *Woods Hole Oceanographic Institution Reference No. 66-34*, 55 pp.

Cawood, P. A., McCausland, P. J. A., and Dunning, G. R. (2001). Opening Iapetus: Constraints from the Laurentian margin in Newfoundland. *Geological Society of America, 113*, 443-453.

Chow, N., and James, N. P. Cambrian Grand Cycles: A northern Appalachian perspective. *Geological Society of America Bulletin, 98*, 418-429.

Cooper, R. A., Nowlan, G. S., and Williams, S. H. (2001). Global Stratotype Section and Point for base of the Ordovician System. *Episodes, 24*, 19-28.

Dahl, T. W., Boyle, R. A., Canfield, D. E., Connelly, J. N., Gill, B. C., Lenton, T. M., and Bizzarro, M. (2014). Uranium isotopes distinguish two geochemically distinct stages during the later Cambrian SPICE event. *Earth and Planetary Science Letters, 401*, 313-326.

Didyk, B. M., Simoneit, B. R. T., Brassell, S. C., and Eglinton, G. (1978). Organic geochemical indicators of palaeoenvironmental conditions of sedimentation. *Nature, 272,* 216-222.

Douglas, A. G., and Eglinton, G. (1966). The distribution of alkanes. In: Swain, T. (Ed.), *Comparative Phytochemistry* (pp. 57-78). London, UK: Academic Press.

Dutta, S., Greenwood, P. F., Brocke, R., Schaefer, R. G., and Mann, U. (2006). New insights into the relationship between *Tasmanites* and tricyclic terpenoids. *Organic Geochemistry, 37,* 117-127.

Edwards, C. T., Fike, D. A., Saltzman, M. R., Lu, W., and Lu, Z. Evidence for local and global redox conditions at an Early Ordovician (Tremadocian) mass extinction. *Earth and Planetary Science Letters, 481,* 125-135.

Elrick, M., Rieboldt, S., Saltzman, M., and McKay, R. M. (2011). Oxygen-isotope trends and seawater temperature changes across the Late Cambrian Steptoean positive carbon-isotope excursion (SPICE event). *Geology, 39,* 987-990.

Eglinton, G., and Hamilton, R. J. (1967). Leaf epicuticular waxes. *Science, 156,* 1322-1335.

Fang, R., Littke, R., Zieger, L., Baniasad, A., Li, M., and Schwarzbauer, J. (2019). Changes of composition and content of tricyclic terpane, hopane, sterane, and aromatic biomarkers throughout the oil window: A detailed study on maturity parameters of Lower Toarcian Posidonia Shales of the Hils Syncline, NW Germany. *Organic Geochemistry, 138,* 1-19.

Farrimond, P., Bevan, J. C., Bishop, A. N. (1999). Tricyclic terpane maturity parameters: response to heating by an igneous intrusion. *Organic Geochemistry, 30*, 1011-1019.

Farrimond, P., Talbot, H. M., Watson, D. F., Schulz, L. K., and Wilhelms, A. (2004). Methylhopanoids: Molecular indicators of ancient bacteria and a petroleum correlation tool. *Geochimica et Cosmochimica Acta, 68*, 3873-3882.

Ferrer, F. M., Bailey, J. V., Corsetti, F., Moldowan, J. M., Barbanti, S. M., Caron, D., Bryant-Huppert, J. (2018). Assessing biomarker syngeneity: An in-situ approach using monoclonal antibodies. *Organic Geochemistry, 124*, 112-122.

Fox, D. (2016). What sparked the Cambrian explosion? *Nature, 530*, 268-270.

Galarraga, F., Reategui, K., Martinez, A., Martinez, M., Llamas, J. F., and Marquez, G. (2008). V/Ni ratio as a parameter in palaeoenvironmental characterisation of nonmature medium-crude oils from several Latin American basins. *Journal of Petroleum Science and Engineering, 61*, 9-14.

Gill, B. C., Lyons, T. W., Young, S. A., Kump, L. R., Knoll, A. H., and Saltzman, M. R. (2011). Geochemical evidence for widespread euxinia in the Later Cambrian ocean. *Nature, 469*, 80-83.

Glumac, B., and Walker, K. R. (1998). A Late Cambrian positive carbon-isotope excursion in the Southern Appalachians; relation to biostratigraphy, sequence stratigraphy, environments of deposition, and diagenesis. *Journal of Sedimentary Research, 68*, 1212-1222.

Greenwood, P. F., Arouri, K. R., and George, S. C. (2000). Tricyclic terpenoid composition of *Tasmanites* kerogen as determined by pyrolysis GC-MS. *Geochimica et Cosmochimica Acta, 64*, 1249-1263.

Harvey, H. R., and McManus, G. B. (1991). Marine ciliates as a widespread source of tetrahymanol and hopan-3β-ol in sediments. *Geochimica et Cosmochimica Acta, 55*, 3387-3390.

Heissler, D., and Ladenburger, C. (1988). Synthesis of (+) – tricyclohexaprenol, a possible precursor of a family of tricyclic geoterpanes, and synthesis of an isomer. *Tetrahedron, 44*, 2513-2521.

Hinchey, A. M., Knight, I., Kilfoil, G., and Hicks, L. (2015). Geological overview and hydrocarbon potential of Cambrian-Ordovician strata of the outer Humber zone, western Newfoundland. *Geological Survey Report, 15*, 143-171.

Huang, W-Y., Meinschein, W. G. (1979). Sterols as ecological indicators. *Geochemica et Cosmochimica Acta, 43*, 739-745.

James, N. P., and Stevens, R. K. (1986). Stratigraphy and Correlation of the Cambro-Ordovician Cow Head Group, western Newfoundland. *Geological Survey of Canada, 366*, 1-143.

James, N. P., Stevens, R. K., Barnes, C. R., and Knight, I. Evolution of a Lower Paleozoic continental-margin carbonate platform, northern Canadian Appalachians. *The Society of Economic Paleontologists and Mineralogists, Special Publication, 44*, 123-146.

Johns, W. D. (1979). Clay mineral catalysis and petroleum generation. *Annual Review of Earth and Planetary Sciences, 7,* 183-198.

Kleemann, G., Poralla, K., Englert, G., Kjøsen, H., Liaaen-Jensen, S., Neunlist, S., and Rohmer, M. (1990). Tetrahymanol from the phototropic bacterium *Rhodopseudomonas palustris*: first report of a gammacerane triterpene from a prokaryote. *Journal of General Microbiology, 136,* 2551-2553.

Klinkhammer, G. P., and Palmer, M. R. (1991). Uranium in the oceans: where it goes and why. *Geochimica et Cosmochimica Acta, 55,* 1799-1806.

Krajewski-Bertrand, M.-A., Hayer, M., Wolff, G., Milon, A., Albrecht, A.-M., Heissler, D., Nakatani, Y., and Ourisson, G. (1990). Tricyclohexaprenol and an octaprenediol, two of the "primitive" amphiphilic lipids do improve phospholipidic membranes. *Tetrahedron, 46,* 3143-3154.

Landing, E. (2013). The Great American Carbonate Bank in Eastern Laurentia: Its Births, Deaths, and Linkage to Paleooceanic Oxygenation (Early Cambrian – Late Ordovician). *The American Association of Petroleum Geologists, 98,* 451-492.

Lavoie, D., Desrochers, A., Dix, G., Knight, I., and Hersi, O. S. (2012). The Great American Carbonate Bank in Easter Canada: An Overview. *The American Association of Petroleum Geologists, 98,* 499-523.

LeRoy, M. A., and Gill, B. C. (2019). Evidence for the development of local anoxia during the Cambrian SPICE event in eastern North America. *Geobiology, 17,* 381-400.

Li, D., Zhang, X., Chen, K., Zhang, G., Chen, X., Huang, W., Peng, S., and Shen, Y. (2017). High-resolution C-isotope chemostratigraphy of the uppermost Cambrian stage (Stage 10) in South China: implications for defining the base of Stage 10 and palaeoenvironmental change. *Geological Magazine, 1*, 1-12.

Matys, E. D., Mackey, T., Grettenberger, C., Mueller, E., Summer, D. Y., Hawes, I., and Summons, R. E. (2019). Bacteriohopanepolyols across environmental gradients in Lake Vanda, Antarctica. *Geobiology,* 1-12.

Miller, J. F., Repetski, J. E., Nicoll, R. S., Nowlan, G., and Ethington, R. L. (2014). The conodont Iapetognathus and its value for defining the base of the Ordovician System. *GFF, 136*, 185-188.

Moldowan, J. M., Seifert, W. K., and Gallegos, E. J. (1983). Identification of an extended series of tricyclic terpanes in petroleum. *Geochimica et Cosmochimica Acta, 47*, 1531-1534.

Moldowan, J. M., Seifert, W. K., and Gallegos, E. J. (1985). Relationship Between Petroleum Composition and Depositional Environment of Petroleum Source Rocks. *The American Association of Petroleum Geologists Bulletin, 69*, 1255-1268.

Neunlist, S., and Rohmer, M. (1985). Novel hopanoids from the methylotrophic bacteria *Methylococcus capsulatus* and *Methylomonas methanica*. *Journal of Biochemistry, 231*, 635-639.

Ourisson, G., Albrecht, P., and Rohmer, M. (1979). The hopanoids. Paleochemistry and biochemistry of a group of natural products. *Pure and Applied Chemistry, 51*, 709-729.

Ourisson, G., Albrecht, P., and Rohmer, M. (1984). The microbial origin of fossil fuels. *Scientific American, 251*, 44-51.

Palmer, A. R. (1984). The Biomere problem: Evolution of an idea. *Journal of Paleontology, 58*, 599-611.

Perfetta, P. J., Shelton, K. L., and Stitt, J. H. (1999). Carbon isotope evidence for deep-water invasion at the Marjumiid-Pterocephaliid biomere boundary, Black Hills, USA: a common origin for biotic crises on Late Cambrian shelves. *Geology*, *27*, 403-406.

Peters, K. E., and Moldowan, J. M. (1991). Effects on source, thermal maturity, and biodegradation on the distribution and isomerization of homohopanes in petroleum. *Organic Geochemistry, 17*, 47-61.

Peters, K. E., Walters, C. C., and Moldowan, J. M. (2005). *The Biomarker Guide* (2nd vol.). New York, NY: Cambridge University Press.

Powell, T. G., and McKirdy, D. M. (1973). Relationship between Ratio of Pristane to Phytane, Crude Oil Composition and Geological Environment in Australia. *Nature Physical Science, 243*, 37-39.

Rashby, S. E., Sessions, A. L., Summons, R. E., and Newman, D. K. (2007). Biosynthesis of 2-methylbacteriohopanepolyols by an anoxygenic phototroph. *Proceedings of the National Academy of Sciences, 104*, 15099-15104.

Retallack, G. J. (2000). Ordovician life on land and early Paleozoic global change. *The Paleontological Society Papers, 6*, 21-46.

Ripperdan, R. L., Magaritz, M., Nicoll, R. S., and Shergold, J. H. (1992). Simultaneous changes in carbon isotopes, sea level, and conodont biozones within the Cambrian-Ordovician boundary interval at Black Mountain, Australia. *Geology, 20*, 1039-1041.

Rohmer, M., Bisseret, P., and Sutter, B. (1991). The hopanoids, bacterial triterpenoids, and the biosynthesis of isoprenic units in prokaryotes. In: *Progress in Drug Research, 37*, 271-285.

Salamon, M. A., Gerrienne, P., Steemans, P., Gorzelak, P., Filipiak, P., Le Hérissé, Paris, F., Cascales-Miñana, Brachaniec, T., Misz-Kennan, M., Niedźwiedzki, and Trela, W. (2018). *Letters*, 1305-1309.

Saltzman, M. R., Cowan, C. A., Runkel, A. C., Runnegar, B., Stewart, M. C., and Palmer, A. R. (2004). The Late Cambrian SPICE ($\delta^{13}C$) event and the Sauk II-Sauk III regression; new evidence from Laurentian basins in Utah, Iowa, and Newfoundland. *Journal of Sedimentary Research, 74*, 366-377.

Saltzman, M. R., Edwards, C. T., Adrain, J. M., and Westrop, S. R. (2015). Persistent oceanic anoxia and elevated extinction rates separate the Cambrian and Ordovician radiations. *Geology, 43*, 807-810.

Saltzman, M. R., Ripperdan, R. L., Brasier, M. D., Lohmann, K. C., Robison, R. A., Chang, W. T., Peng, S., Ergaliev, E. K., and Runnegar, B. (2000). A global carbon isotope excursion (SPICE) during the Late Cambrian: relation to trilobite extinctions, organic-matter burial and sea level. *Palaeogeography, Palaeoclimatology, Palaeoecology, 162*, 211-223.

Saltzman, M. R., Runnegar, B., Lohmann, K. C. (1998). Carbon isotope stratigraphy of Upper Cambrian (Steptoean Stage) sequences of the eastern Great Basin: Record of a global oceanographic event. *Geological Society of America Bulletin, 110*, 285-297.

Sefein, K. J., Nguyen, T. X., Paul Philp, R. (2017). Organic geochemical and paleoenvironmental characterization of the Brown Shale Formation, Kilira sub-basin, Central Sumatra Basin, Indonesia. *Organic Geochemistry, 112*, 137-157.

Seifert, W. K., and Moldowan, J. M. (1978). Applications of steranes, terpanes, and monoaromatics to the maturation, migration, and source of crude oils. *Geochimica et Cosmochimica Acta, 42*, 77-95.

Seifert, W. K. and Moldowan, J. M. (1986). Use of biological markers in petroleum exploration. In: *Methods in Geochemistry and Geophysics* (R. B. Johns, ed.) Vol. 24., 261-290.

Sela-Adler, M., Ronen, Z., Herut, B., Antler, G., Vigderovich, H., Eckert, W., and Sivan, O. (2017). Co-existence of Methanogenesis and Sulfate Reduction with Common Substrates in Sulfate-Rich Estuarine Sediments. *Frontiers in Microbiology, 8*, 1-11.

Sial, A. N., Peralta, S., Gaucher, C., Alfonso, R. N., and Pimentel, M. A. (2008). Upper Cambrian carbonate sequences of the Argentine Precordillera and the Steptoean C-isotope positive excursion (SPICE). *Gondwana Research, 13*, 437-452.

Sinninghe Damasté, J. S., Kenig, F., Koopmans, M. P., Köster, J., Schouten, S., Hayes, J. M., De Leeuw, J. W. (1995). Evidence for gammacerane as an indicator of water column stratification. *Geochimica et Cosmochimica Acta, 59*, 1895-1900.

Socorro, J., and Maurrasse, F. J-M. R. (2016). Continuous episodic dysoxia related to OAE1A, Organyà Basin, El Pujal section, Catalunya, northeast Spain. *Geological Society of America,* abstract.

Socorro, J., Maurrasse, F. J-M. R., Sanchez-Hernandez, Y. (2017). Characterization of the negative carbon isotope shift in segment C2, its global implications as a harbinger of OAE1a. *Science China Earth Sciences, 60*, 30-43.

Spencer, R. J., and Demicco, R. V. (2002). Facies and sequence stratigraphy of two Cambrian grand cycles: implications for Cambrian sea level and origin of grand cycles. *Bulletin of Canadian Petroleum Geology, 50*, 478-491.

Summons, R. E., Jahnke, L. L., and Roksandic, Z. (1994). Carbon isotopic fractionation in lipids from methanotrophic bacteria: Relevance for interpretation of the geochemical record of biomarkers. *Geochimica et Cosmochimica Acta, 58*, 2853-2863.

Summons, R. E., Jahnke, L. L., Hope, J. M., and Logan, G. A. (1999). 2-Methylhopanoids as biomarkers for cyanobacterial oxygenic photosynthesis. *Nature, 400*, 554-557.

Summons, R. E., and Walter, M. R. (1990). Molecular fossils and microfossils of prokaryotes and protists from Proterozoic sediments. *American Journal of Science, 290-A*, 212-244.

Ten Haven, H. L., Rohmer, M., Rullkötter, and Bisseret, P. (1989). Tetrahymanol, the most likely precursor of gammacerane, occurs ubiquitously in marine sediments. *Geochimica et Cosmochimica Acta, 53*, 3073-3079.

Tribovillard, N., Algeo, T. J., Lyons, T., and Riboulleau, A. (2006). Trace metals as paleoredox and paleoproductivity proxies: An update. *Chemical Geology, 232*, 12-32.

Valentine, J. W., Jablonski, D., and Erwin, D. H. Fossils, molecules and embryos: new perspectives on the Cambrian explosion. *Development, 126*, 852-859.

Venkatesan, M. I. (1989). Tetrahymanol: Its widespread occurrence and geochemical significance. *Geochimica et Cosmochimica Acta, 53*, 3095-3101.

Ventura, G. T., Hall, G. J., Nelson, R. K., Frysinger, G. S., Raghuraman, B., Pomerantz, A. E., Mullins, O. C., and Reddy, C. M. (2011). Analysis of petroleum compositional similarity using multiway principal components analysis (MPCA) with comprehensive two-dimensional gas chromatographic data. *Journal of Chromatography A, 1218*, 2584-2592.

Ventura, G. T., and MacRae, A. (2019). *Attenuation of Petroleum Generation Characteristics by the Sulfurization of Organic Matter in Westphaflan Carboniferous Lacustrine Source Rocks: A Geochemical Study of Potential*

*Marine Incursions* (OERA Report). Halifax, NS: Saint Mary's University, Department of Geology.

Volkman, J. K. (1986). A review of sterol markers for marine and terrigenous organic matter. *Organic Geochemistry, 9,* 83-99.

Waldron, J. W. F., and Stockmal, G. S. (1994). Structural and tectonic evolution of the Humber Zone, western Newfoundland: A regional model for Acadian thrust tectonics. *Tectonics, 13,* 1498-1513.

Wang, L., and Azmy, K. (2019). Palaeoenvironmental changes in slope carbonates across the Late Cambrian-Early Ordovician in western Newfoundland. *Geological Journal,* 1-13.

Welander, P. V., and Summons, R. E. (2012). Discovery, taxonomic distribution, and phenotypic characterization of a gene required for 3-methylhopanoid production. *Proceedings of the National Academy of Sciences, 109,* 12905-12910.

Yoda, M., Kitagawa, M., and Miyaji, Y. (1987). Long term competition between sulfate-reducing and methane-producing bacteria for acetate in anaerobic biofilm. *Water Research, 21,* 1547-1556.